VON KARMAN INSTITUTE FOR FLUID DYNAMICS

LECTURE SERIES 1988-04

INTAKE AERODYNAMICS

FEBRUARY 22 - 26, 1988

CFD APPLICATION TO SUPERSONIC/HYPERSONIC INLET AIRFRAME INTEGRATION

Thomas J. Benson
NASA-Lewis Research Center, Ohio, USA

CFD APPLICATION TO SUPERSONIC HYPERSONIC INLET AIRFRAME INTEGRATION

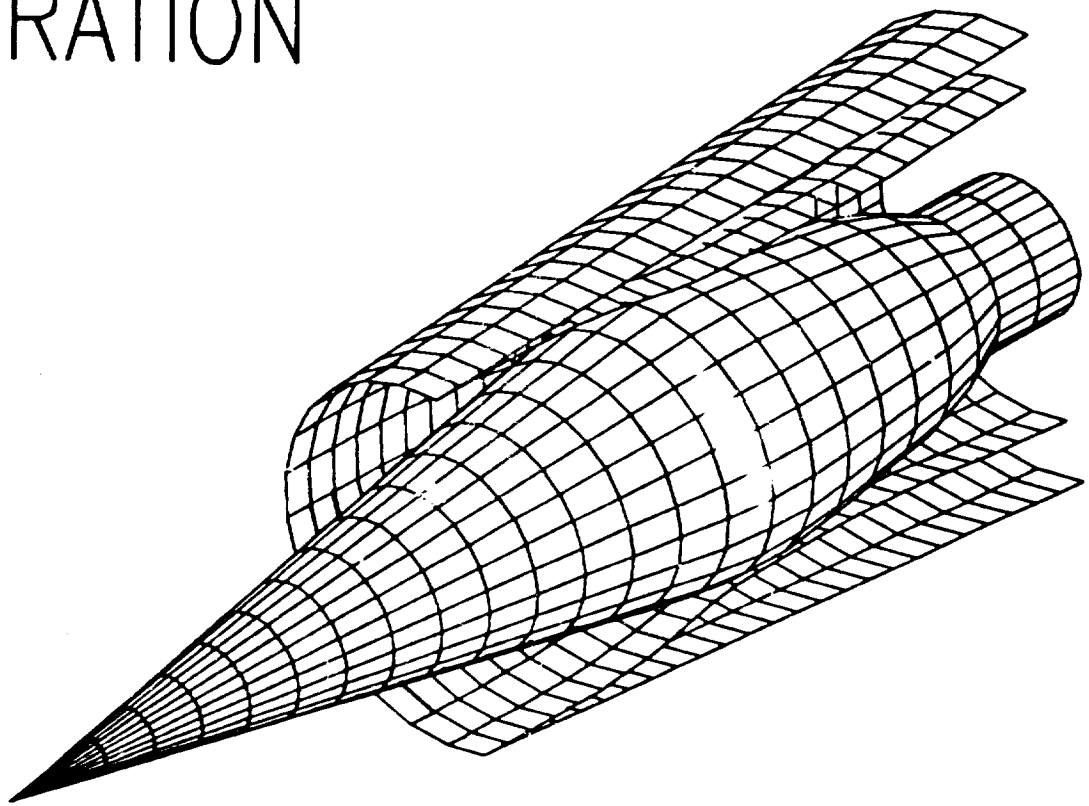

Thomas J. Benson
Senior Research Engineer
NASA Lewis Research Center – Cleveland Ohio – USA

FUTURE REGIME

The operating envelope for future high Mach number aircraft is shown on this figure compared to the regime for current aircraft (shaded area). The area of interest for this paper is Mach 2.5 to 6.0, where advanced technology turbofan/turbojet (Mach<4.0) and turboramjet (4.0<M<6.0) propulsion systems are being condsidered. The aircraft applications include military weapons systems for both defensive and offensive missions and comerical transports.

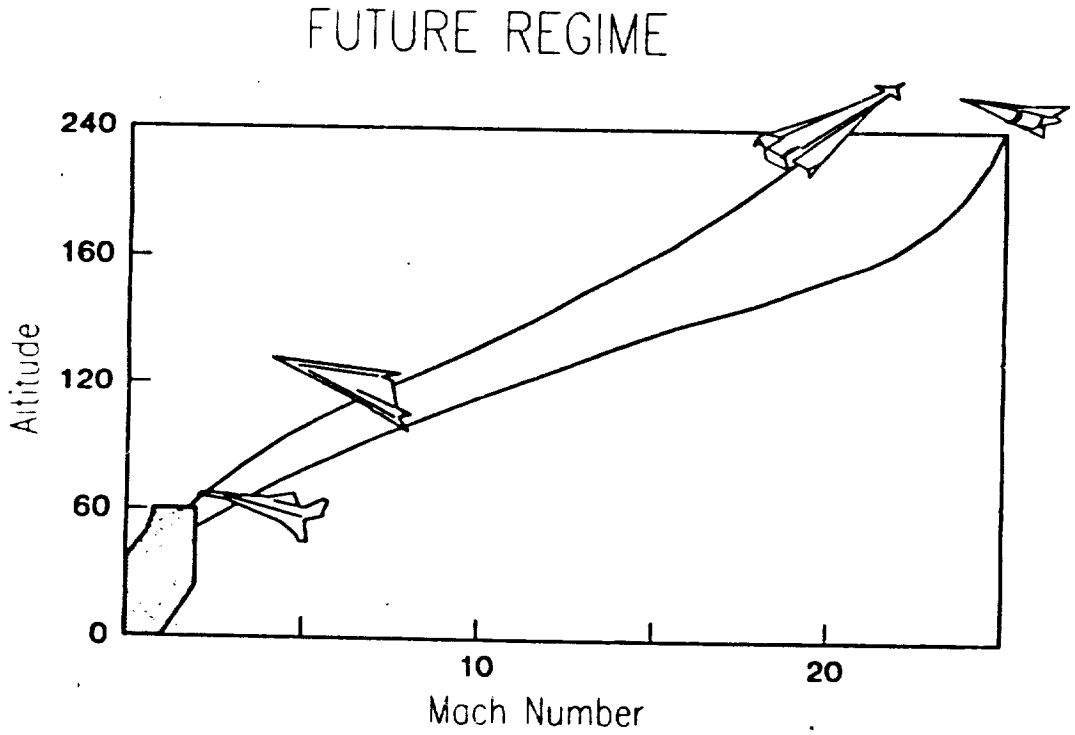

CFD FOR INLET AIRFRAME INTEGRATION

Developing Insight and Understanding

Computational Fluid Dynamics (CFD) is becoming an increasingly powerful tool in the aerodynamic design of aerospace systems, owing to improvements in numerical algorithms, geometric modeling, grid generation, and physical parameter modeling, as well as dramatic improvements in supercomputer processing speed and memory. With the realization of the potential of forthcoming supercomputers, much of the current CFD work will expand to address more complex configurations, geometries, flight regimes, and applications, while some of the existing work will become components of more complex systems of solutions to problems of modeling, grid generation, flow field solution, and flow visualization. Computational Fluid Dynamics is also being used extensively throughout the propulsion community because of a lack of alternatives for achieving insight into the basic controlling mechanisms of the complicated, highly coupled interacting aspects of propulsion fluid dynamics. Thus CFD will become an important aerospace design and development tool requiring a high level of confidence.

To meet the required confidence level, the existing and forthcoming CFD application codes must be verified and validated with the best available experimental data. Because of the complexity of the aerodynamic flows that will be routinely computed, the experimental data base must expand to include not only surface-measurable quantities, but also detailed measurements of fluid and thermal parameters throughout the flow regime of interest. These focused experimental test clearly require detailed flow quantity measurements in addition to integral checks. Also, the errors inherent in experimental testing must be identified, understood, and minimized in order to produce the high-quality, accurate benchmark data that are required for validation of complex CFD applications codes and for use in developing physical modeling data for complex flows.

The concept of "benchmark" or "validation" experiments that highlight one or more basic flow mechanisms important to the inlet airframe system also affords the design engineer the opportunity to study and understand highly complex three dimensional viscous flows from a building block concept, i.e., highly complex viscous flows are composed of "fundamental" or "benchmark" phenomena which interact with each other. With close interaction between CFD and experimentation, advanced computer programs will be used both to design an experiment and to predict the results so that the the test, or design, is under control at all times. But this interaction also gives the researcher a fundamental understanding of the fluid processes that are important to the inlet airframe system under design. This idea is the main thrust of this seminar series on a User's Technology Guide to CFD Inlet Airframe Integration.

CFD FOR INLET AIRFRAME INTEGRATION
Developing Insight and Understanding

"The complementary interplay of CFD and experiment is especially important in the modern world of tailored designs, where the goal is not to generate half-blind global correlations, but to prove the accuracy of a total design system by means of benchmark demonstrations in reliable facilities"

Current Capabilities and Future Direction
in
Computational Fluid Dynamics

CATEGORIES OF CFD-RELATED EXPERIMENTS

Four categories of experimentation were recognized by the Ad Hoc Committee on CFD Validation, NASA Aeronautics Advisory Committee, to be intimately associated with the development of CFD capability, namely

A. Experiments designed to understand flow physics

B. Experiments designed to develop physical models for CFD codes

C. Experiments designed to calibrate CFD codes

D. Experiments designed to validate CFD codes

All four catagories of experiments are important and are necessary to build a mature CFD capability. Validation experiments should only be a part of the total experimental focus and should be formulated to provide specific data for validating CFD codes.

Equally important for validation is the mapping of the CFD code's sensitivity to numerical algorithms, grid density, and physical models. These effects must be known to the same degree as experimental accuracy and resolution in order to understand the applicability of the code over a wide range of flow parameters. This is particular important to the design engineer, who must often rely on computer studies to make a design decision.

CATEGORIES OF CFD-RELATED EXPERIMENTS

A. Experiments designed to understand flow physics

B. Experiments designed to develop physical models for CFD codes

C. Experiments designed to calibrate CFD codes

D. Experiments designed to validate CFD codes

The Ad Hoc Committee on CFD Code Validation
NASA Aeronautics Advisory Committee

CFD CODE VALIDATION DEFINITION

"Detailed surface-and-flow-field comparisons with experimental data to verify the codes ability to accurately model the critical physics of the flow. Validation can occur only when the accuracy and limitations of the experimental data are known and throughly understood and when the accuracy and limitations of the codes numerical algorithms, grid density effects, and physical basis are equally known and understood over a range of specified parameters."

The Ad Hoc Committee on CFD Code Validation
NASA Aeronautics Advisory Committee

SUPERSONIC INLET TYPES

For supersonic aircraft with flight Mach numbers less than 6.0, the inlet must slow the incoming supersonic airstream to subsonic conditions for turbojet or ramjet operation. This slowing of the flow must be accomplished with a minimum amount of drag, total energy (pressure) loss, and flow distortion. The flow is typically brought from supersonic to subsonic conditions by a system of shock waves generated by the inlet, then further slowed in a subsonic diffuser to the engine face.

As shown in the figure, the simplest inlet is a pitot, or normal shock, inlet in which the flow is slowed to subsonic conditions by a single normal shock. This type of inlet works quite well at very low supersonic Mach numbers, but for speeds above Mach 1.5, the total pressure loss through the normal shock seriously degrades performance. The external compression inlet counteracts this loss in total pressure by passing the airstream through several weak oblique shocks before it encounters the normal, or terminal shock. Through each oblique shock the Mach number is reduced and some total pressure is lost. The total pressure loss through the terminal shock is greatly reduced, however, due to the lower Mach number just upstream of this shock. The net effect is an inlet with increased total pressure recovery when compared with a simple pitot inlet; the more oblique shocks present in the external compression inlet, the higher the recovery. As the Mach number increases above 2.5, the number and strength of the oblique shocks increases with a corresponding decrease in pressure recovery. The compression system must be longer and therefore heavier and the drag associated with turning the flow also increases. The mixed compression inlet is able to over come some of these failings by taking the terminal shock inside the inlet duct. Reflecting an oblique shock from the internal surfaces produces multiple weak oblique shocks, higher recovery, lighter weight and less drag. Some of these performance gains are offset by a need to control the interaction of the internal shocks with boundary layers on the surfaces and to insure that the normal shock remains inside the duct.

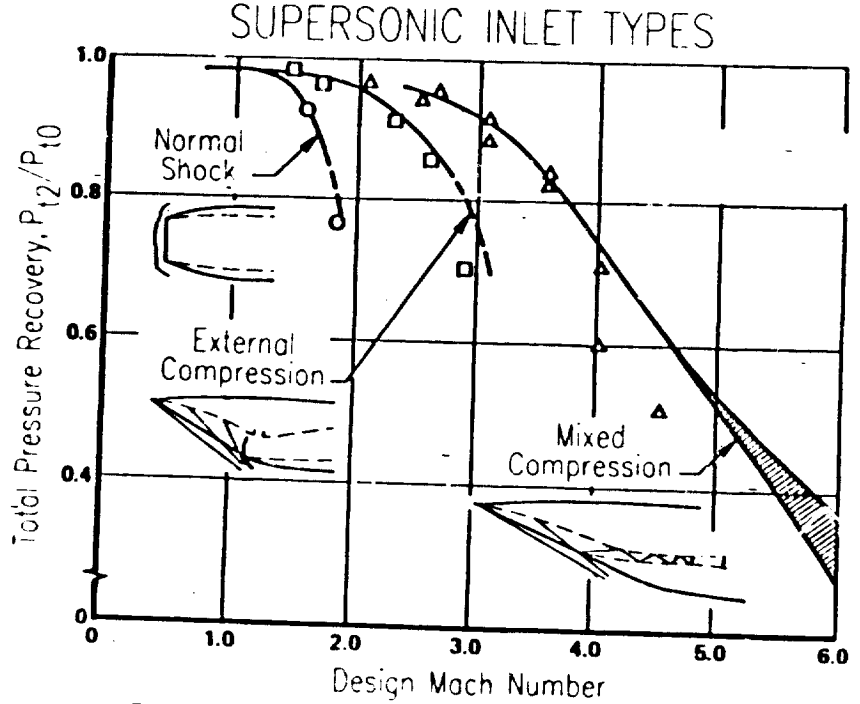

SUPRESONIC EXTERNAL COMPRESSION INLETS

Fundamental Interactions

For external compression inlets, the terminal normal shock remains outside the inlet duct. This figure shows some of the fundamental fluid interactions present near the normal shock. The supersonic flow enters from the left with the ramp compression surfaces at the bottom and the cowl at the top. Boundary layers build up on both ramp and cowl surfaces. The subsonic flow leaves at the right and would then enter the compressor of the engine. The flow transitions from supersonic to subsonic through the normal shock which sits in front of the cowl. This strong shock interacts with the ramp boundary layer, usually resulting in flow separation for terminal Mach numbers greater than 1.3 . To eliminate this separation, a bleed slot or aperutre is present on the ramp surface which uses the pressure generated by the normal shock to drive the separated flow into another duct for disposal overboard. Removing flow through the throat slot creates an expansion fan at the trailing edge of the ramp which interacts with the terminal shock and a free shear layer which impinges on the aft ramp. Since there is a drag penalty for bleeding the boundary layer overboard, the minimum amount of bleed must be carefully determined either experimentally or computationally.

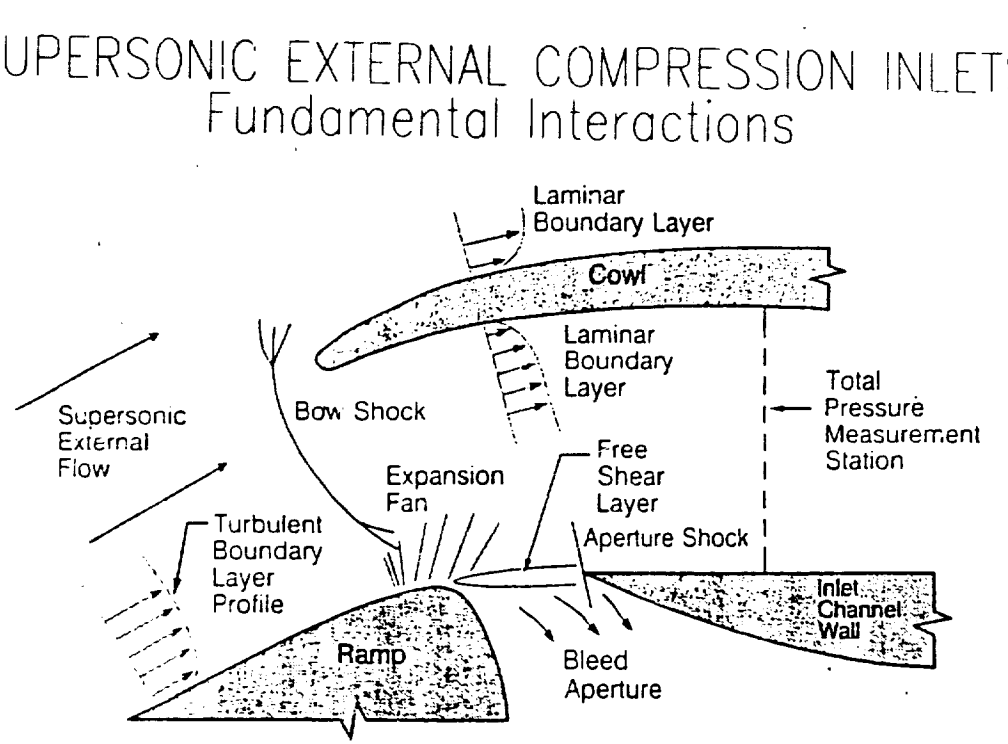

NORMAL SHOCK WAVE BOUNDARY LAYER INTERACTION

Comparision of Analytical with Shadowgraph

This figure shows a comparison of the computed and actual flowfields in the vicinity of the terminal shock of an external compression inlet. Both the experiment and the computer analysis were performed by the Boeing corporation, and have been presented by Campbell (Ref. 57). The computer code used in this analysis is a two dimensional explicit MacCormack solver. On the left is a shadowgraph photo, showing the terminal shock, expansion fan, slip surface and aperture shock. On the right are computed Mach number contours for this configuration. The coalescence of Mach lines corresponds to the terminal and aperture shocks, while the increase in Mach number downstream of the ramp trailing edge correctly corresponds to the expansion fan. The analysis correctly predicts the high speed jet at the aft of the aperture and the shock which occurs within the bleed plenum as seen in the shadowgraph.

NORMAL SHOCK WAVE BOUNDARY LAYER INTERACTION
Comparison of Analytical with Shadowgraph

Shadow Graph

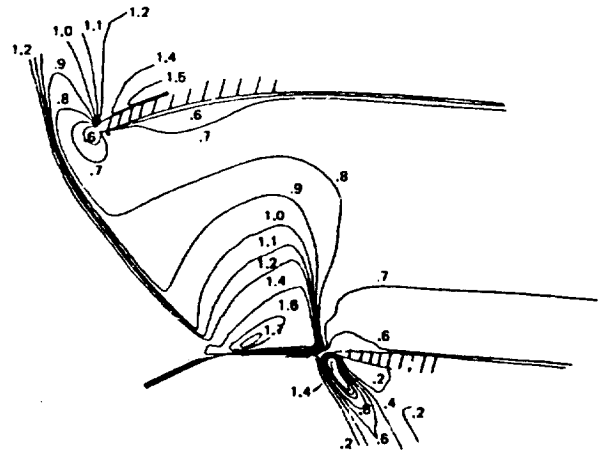

Analytical Mach Contours

SUPERSONIC EXTERNAL COMPRESSION INLETS

Effect of Numerical Diffusion

In the calculation of supersonic flows using central differencing algorithms, one often encounters numerical oscillations in the flow solution. To eliminate these non-physical oscillations and stabilize the solution, various types of artifical viscosity, or numerical diffusion, are used. The amount of numerical diffusion used in the calculation is controlled by a smoothing coefficient. While the numerical diffusion is often necessary to obtain an accurate solution of the problem, great care must be taken to add as little numerical diffusion as required; otherwise, non-physical solutions may result. This figure illustrates some of the problems associated with the use of artificial viscosity. The calculations were done by Campbell (Ref. 57) of Boeing, for the terminal shock problem explained in the previous figure. On the left of the figure are computed Mach number contours which agree quite closely with the experimental results. This calculation was peformed with a low level of artificial viscosity. Increasing the numerical diffusion by a factor of one hundred gives the results shown on the right. The normal shock wave has been thickened and artificially thick boundary layers have been generated on the cowl and ramp surfaces. The interaction of the thickened shock and ramp boundary layer numerically swamps the expansion at the ramp trailing edge. While the calculations contain some of the important physical features, such as the shock waves, boundary layers and slip surface, they miss many of the important details of the physical problem.

SUPERSONIC EXTERNAL COMPRESSION INLETS
Effect of Numerical Diffusion

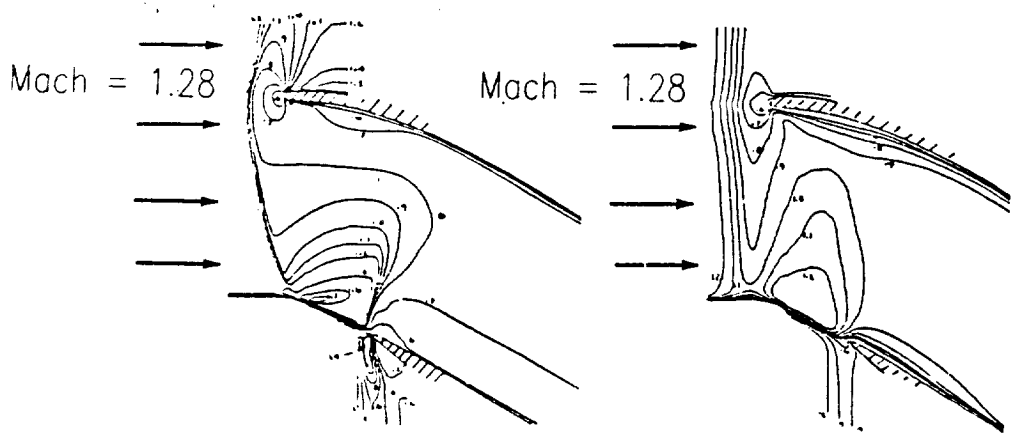

Smoothing Coefficient = 0.5 Smoothing Coefficient = 50.0

SUPERSONIC EXTERNAL COMPRESSION INLETS

Effect of Numerical Diffusion

Total Pressure Profile

While the previous figure showed qualitative effects of numerical diffusion on computed results, this figure gives a quantitative comparison. The figure shows total pressure profiles at the exit of the inlet for three values of the numerical diffusion coefficient. As the coefficient is increased, the boundary layers on both ramp and cowl are artificially thickened. The integrated total pressure would be grossly underpredicted for the largest value of viscosity coefficient. Numerical losses generated by artificial viscosity in the duct would greatly exceed physical losses. Again, great care must exercised in the use of artificaial dissipation.

SUPERSONIC EXTERNAL COMPRESSION INLETS
Effect of Numerical Diffusion
Total Pressure Proflie

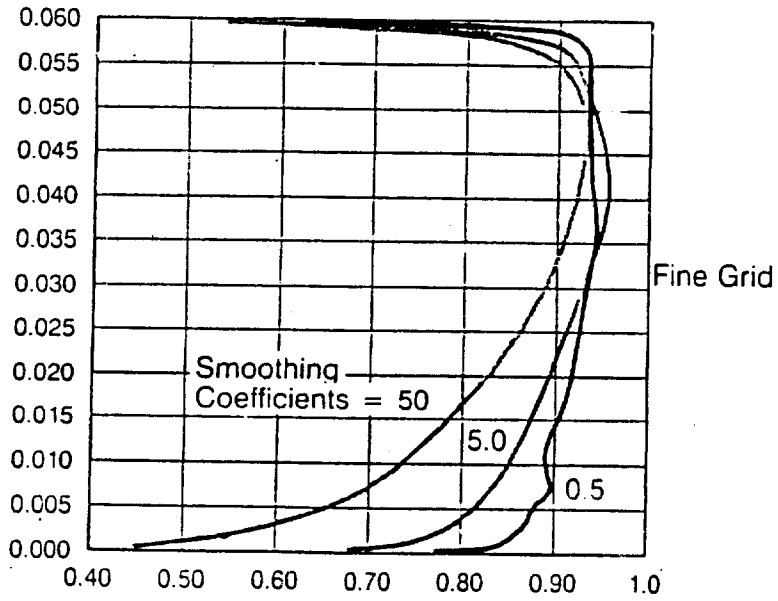

CFD FOR INLET AIRFRAME INTEGRATION

The Benchmark Phenomenon and Code Validation

The goal of providing design analyses tools for supersonic inlet system technology advancement necessitates a two tier experimental validation process to properly evaluate the ability of these three dimensional solvers to predict the relevant flow physics. First, it is necessary to show good predictions of flow parameters of interest to the user community on "generic" configurations which would be typical of real world designs. Such testing should be as realistic as possible. Confidence in the advanced computational capability would increase by leaps and bounds in the user community by this type of demonstration.

A second tier program appears to be called for and here essential elements of these advanced computer design tools would be validated in very simple environments which highlight one or more basic flow mechanisms. The requirements are for overall simplicity and easy access to make the necessary very detailed measurements. Detailed validataion of the codes for the basic flow mechanisms is required through specific benchmark experiments because generic component tests may or may not emphasize any particular basic flow mechanism and overall good agreement may be just that, an "overall" agreement. There may be an unfortunate cancelling effect in the basic flow mechanisms of generic experiments. For instance, one could not analytically investigate the factors affecting inlet performance with any degree of confidence if individual shock wave turbulent boundary layer interactions encountered within the inlet were not well predicted, figure (2). Confidence in making extrapolations using computational tools will increase if the basic mechanisms, when isolated, are predicted both qualitatively and quantitatively.

CFD FOR INLET AIRFRAME INTEGRATION
The Benchmark Phenomenon and Code Validation

"Detailed validation of the code for basic flow mechanisms is required through specific benchmark (validation) experiments because the generic component test may or may not emphasize any particular mechansim, and over all good agreement may be just that....an overall agreement..... For instance, one could not analytically investigate the factors affecting inlet performance with any degree of confidence if the individual shock / wave turbulent boundary layer interactions encountered within the inlet were not well predicted"

Three-Dimensional Viscous Design Methology
of Supersonic Inlet Systems for
Advanced Technology Aircraft

NASA LEWIS 1X1 FT. SUPERSONIC WIND TUNNEL

Facility for Benchmark Flow Studies

To conduct the benchmark validation experiments previously discussed, a small, dedicated facility is required. The NASA Lewis 1X1 foot supersonic research tunnel has been used for many years to study isolated benchmark phenomenon for comparison with CFD analysis. The tunnel has interchangeable nozzle blocks for test section Mach numbers of 1.3, 1.6, 2.0, 2.5, 3.0, 3.5, and 4.0. A heater is currently being added to the tunnel and nozzle blocks exist to study flows at Mach 5.0 and 6.0. The tunnel is a continuous flow facility with air supplied by the central laboratory. Data is recorded and reduced locally and can be archived to the central computer facility at NASA Lewis over the data link. Typical data recorded in the facility include traversing pitot pressure, hot wire, surface static pressure, flow angularity, two component LDV along either axis, as well as schlieren and surface oil flow visualization. The tunnel has provisions for boundary layer bleed and blowing studies.

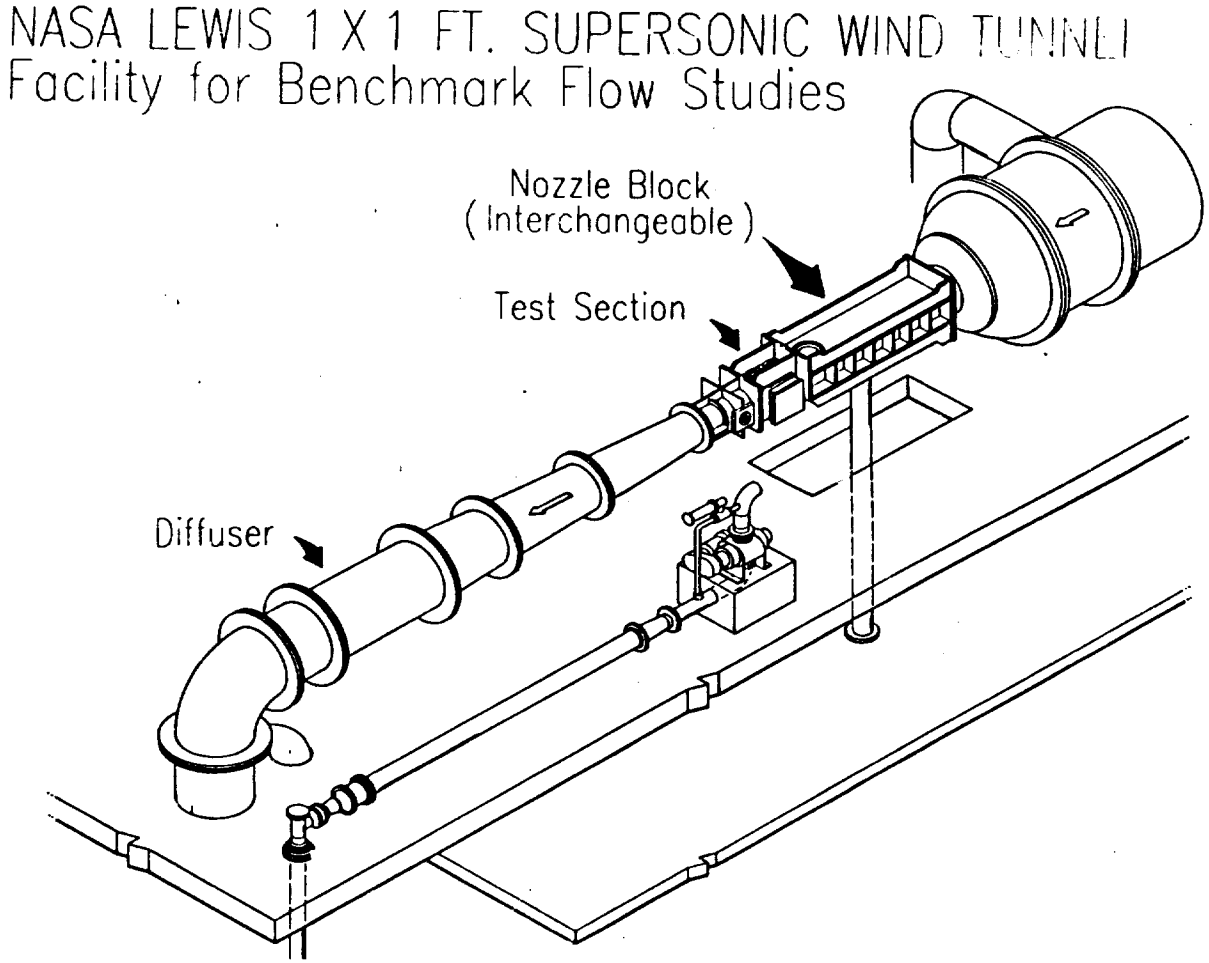

MACH 1.3 NORMAL SHOCK WAVE TURBULENT BOUNDARY LAYER INTERACTION

Comparision of LDV Experiment and Analysis

The fundamental interaction of a normal shock and a boundary layer has been studied at NASA Lewis Research Center. Such an interaction would occur in the terminal shock region of an external or mixed compression inlet. The experiment was performed in the 1X1 supersonic tunnel, while the analysis is a two-dimensional Navier-Stokes solution. The experimental results were obtained with a two component LDV system, while the analysis solves the equations using an efficient LBI scheme. This figure shows a comparison of CFD analysis and experimental results for a Mach 1.3 normal shock/boundary layer interaction. The figure shows Mach number contours through the interaction, with the concentration of contour lines at the top and bottom indicate the wall boundary layer while the verticle concentration indicates the normal shock location. The analysis correctly predicts features seen in the experiment, including the thickening of the boundary layer downstream of the shock, the lamda structure at the base of the shock, the supersonic tongue near the boundary layer but downstream of the shock, and the low Mach number region along the centerline downstream of the shock. The ability of the code to correctly predict this single benchmark interaction gives the engineer confidence in the code's ability to predict similar interactions.

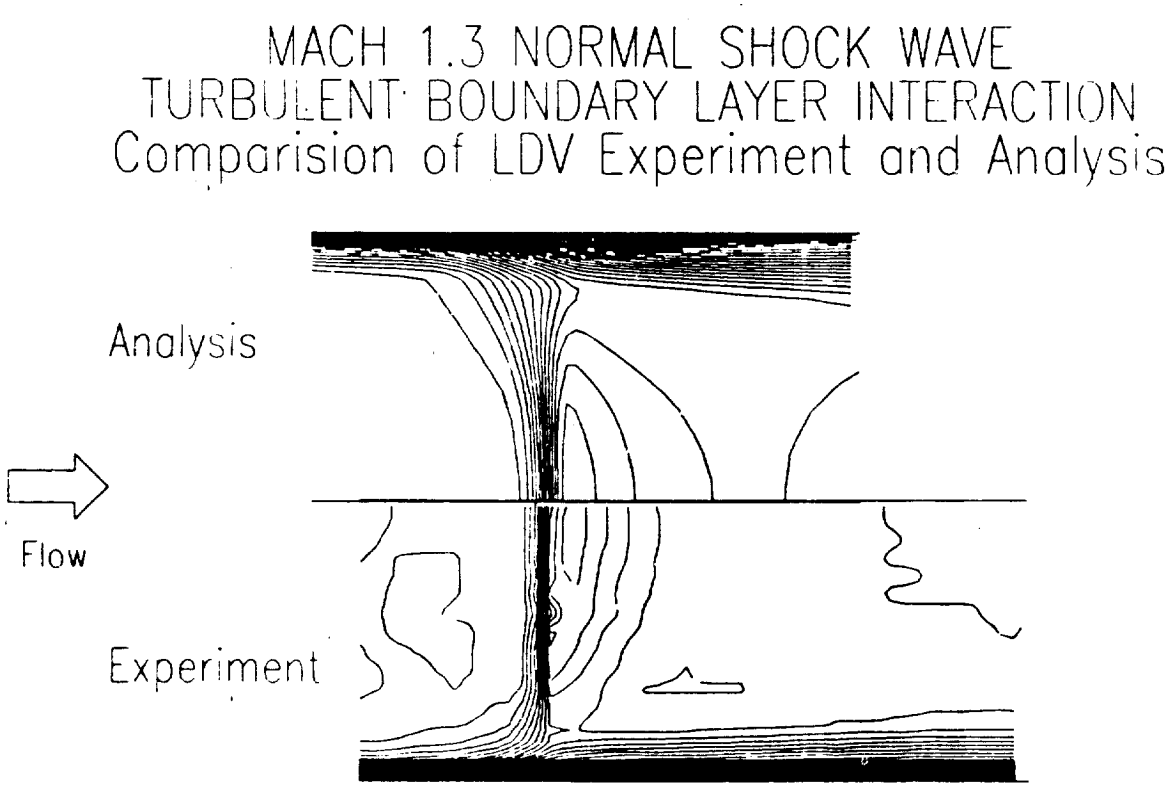

MACH 1.6 NORMAL SHOCK WAVE TURBULENT BOUNDARY LAYER INTERACTION

Comparision of LDV Experiment and Analysis

This figure is quite similar to the previous figure and shows a comparison of analysis and experimental results for a Mach 1.6 normal shock/boundary layer interaction. The analysis and the experimental techniques are the same as that used in the previous figure. The analysis is able to capture many of the features of this interaction; boundary layer thickening, upstream lamda structure, supersonic tongue, and low Mach number packet along the centerline. However, in the experiment, one encounters a re-acceleration of the flow to supersonic conditions and a second weaker normal shock downstream of the primary normal shock. The analysis does not predict this feature because the analysis used is two-dimensional, while the experiment produced large three-dimensional separations in the corners of the wind tunnel. The three-dimensional effects caused the flow to accelerate to supersonic conditions which the two-dimensional analysis could not predict. This computer code is currently be extended to three dimensions and this benchmark interaction will be recomputed to determine if the code correctly predicts the interaction. When using a two-dimensional analysis, one must be sure that the problem is truly two-dimensional; otherwise, incorrect predicitions can occur.

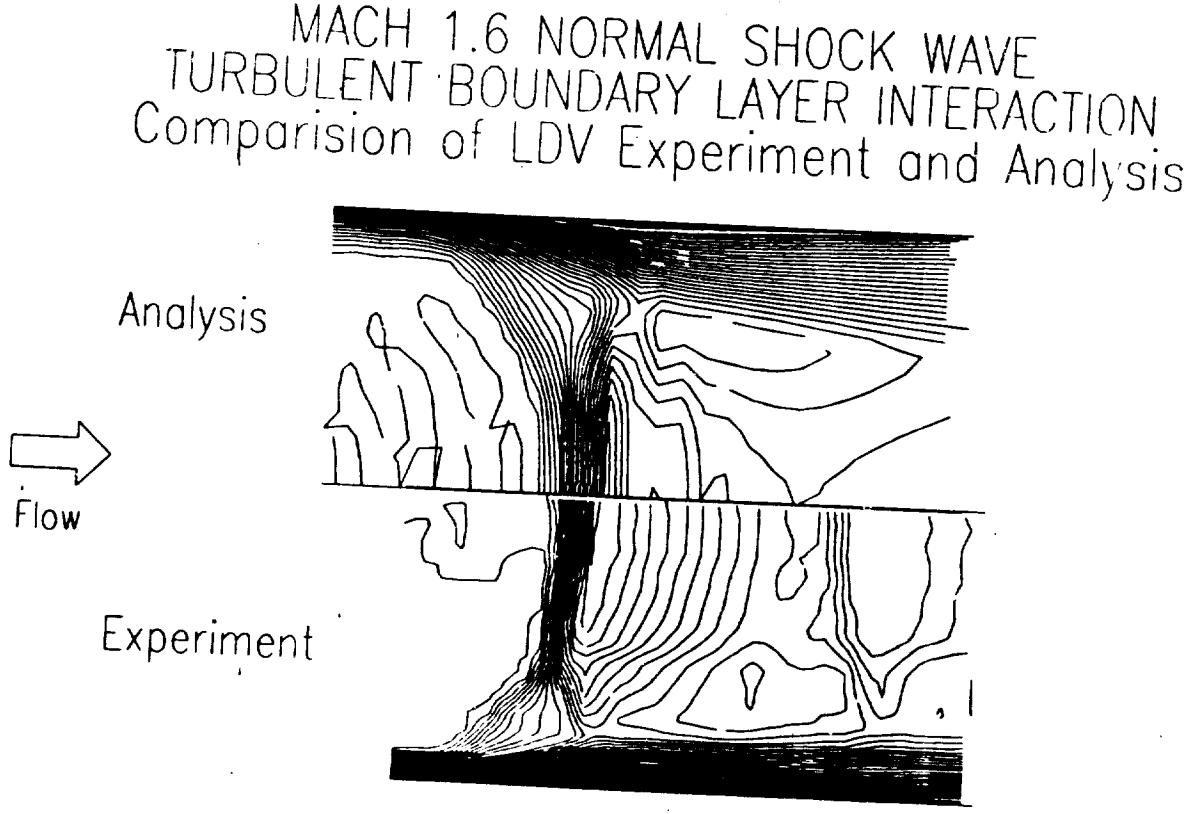

MACH 1.6 NORMAL SHOCK WAVE TURBULENT BOUNDARY LAYER INTERACTION

Schlieren Photograph Showing Lamda Structure

Besides LDV measurements, schlieren photography and surface oil flows were used to study the normal shock boundary layer interaction. This figure shows a schlieren photograph of the flow near the wall for the Mach 1.6 normal shock/boundary layer interaction described in the previous figures. The wall is at the top, and the free stream shock is at the bottom. The characteristic lamda structure is clearly visible. The boundary layer beneath the shock is thickened due to the strong adverse pressure gradient. The displacement effects of the boundary layer cause a small oblique shock to be formed at the base of the normal shock resulting in the lamda structure. This feature was also present in the calculation of this phenomenon.

MACH 1.6 NORMAL SHOCK WAVE
TURBULENT BOUNDARY LAYER INTERACTION
Schlieren Photograph Showing Lamda Structure

MACH 1.6 NORMAL SHOCK WAVE TURBULENT BOUNDARY LAYER INTERACTION

Experimental Oil Flow Patterns

This figure demonstrates the three-dimensional nature of the flow in the Mach 1.6 normal shock/boundary layer interaction. The figure shows oil flow along the walls of the 1X1 supersonic tunnel in the vicinity of the interaction. Large recirculation zones are evident both at the top and bottom corners which introduce three dimensional effects into the flow. The flow along the cenetrline is greatly modified by the recirculation present in the corner of the tunnel.

MACH 1.6 NORMAL SHOCK WAVE
TURBULENT BOUNDARY LAYER INTERACTION
Experimental Oil Flow Patterns

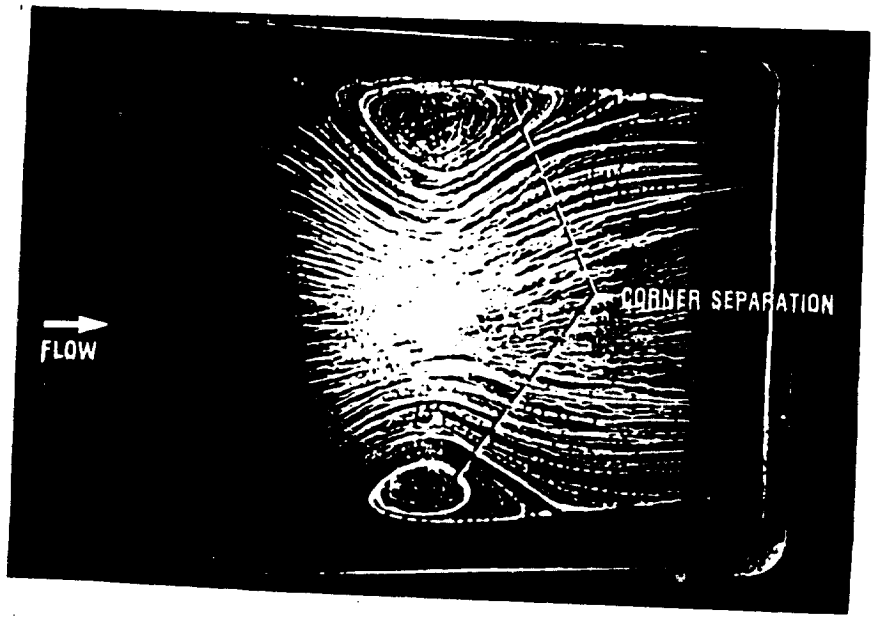

SUPERSONIC EXTERNAL COMPRESSION INLETS

Multi-Region Computational Strategy

Navier Stokes Solution

When calculating full inlets, it is often necessary to divide the computational domain into several regions. This reduces computer in-core storage requirements, and can produce faster solutions if the solution can be physically integrated at differnet rates in different regions. This figure shows a simple two region computational domain for the calculation of flow through an external compression inlet. One region includes flow which passes through the inlet duct, while the other models flow spilled over the cowl. The inlet considered here is the axisymmetric B-58 inlet; the calculations were completed by Howlett and Hunter (Ref. 58) of General Dynamics. Information is passed between the two regions along the line upstream of the cowl lip.

SUPERSONIC EXTERNAL COMPRESSION INLETS
Multi-Region Computational Strategy
Navier Stokes Solution

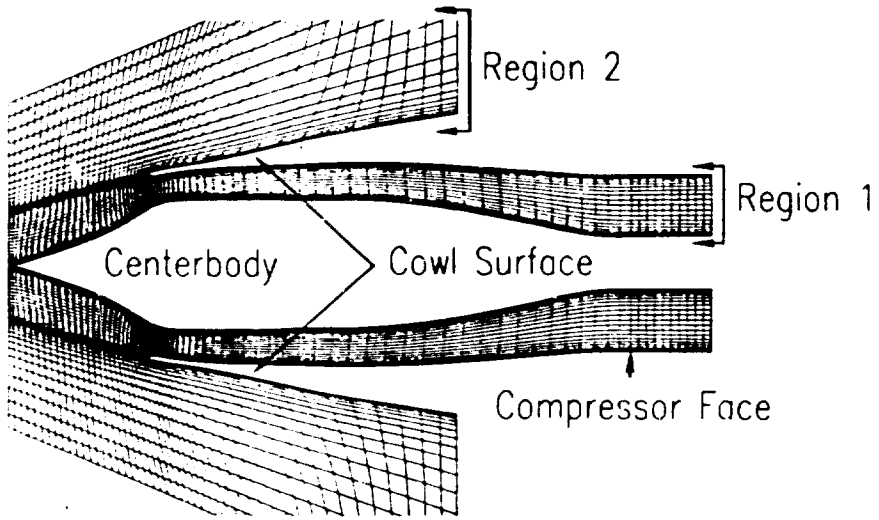

SUPERSONIC EXTERNAL COMPRESSION INLETS

Subcritical to Supercritical Operation

Navier Stokes Solution

This figure shows Navier-Stokes solutions to the flow through the B-58 inlet as calculated by Howlett and Hunter of General Dynamics. The zonal geometry described in the previous figure was used for this calculation. The figure clearly shows the oblique shock generated by the cone, the terminal normal shock for this external compression inlet, and the boundary layer buildup on internal surfaces. Proceeding from the top of the figure to the bottom, the computational flow plug was opened and, corresponding to experimental results, the mass flow ratio is seen to change very little while the recovery decreases in supercritical operation. The normal shock is also seen to move closer to the throat as the flow plug is opened. The continuity of the normal shock across the grid region boundary is evident.

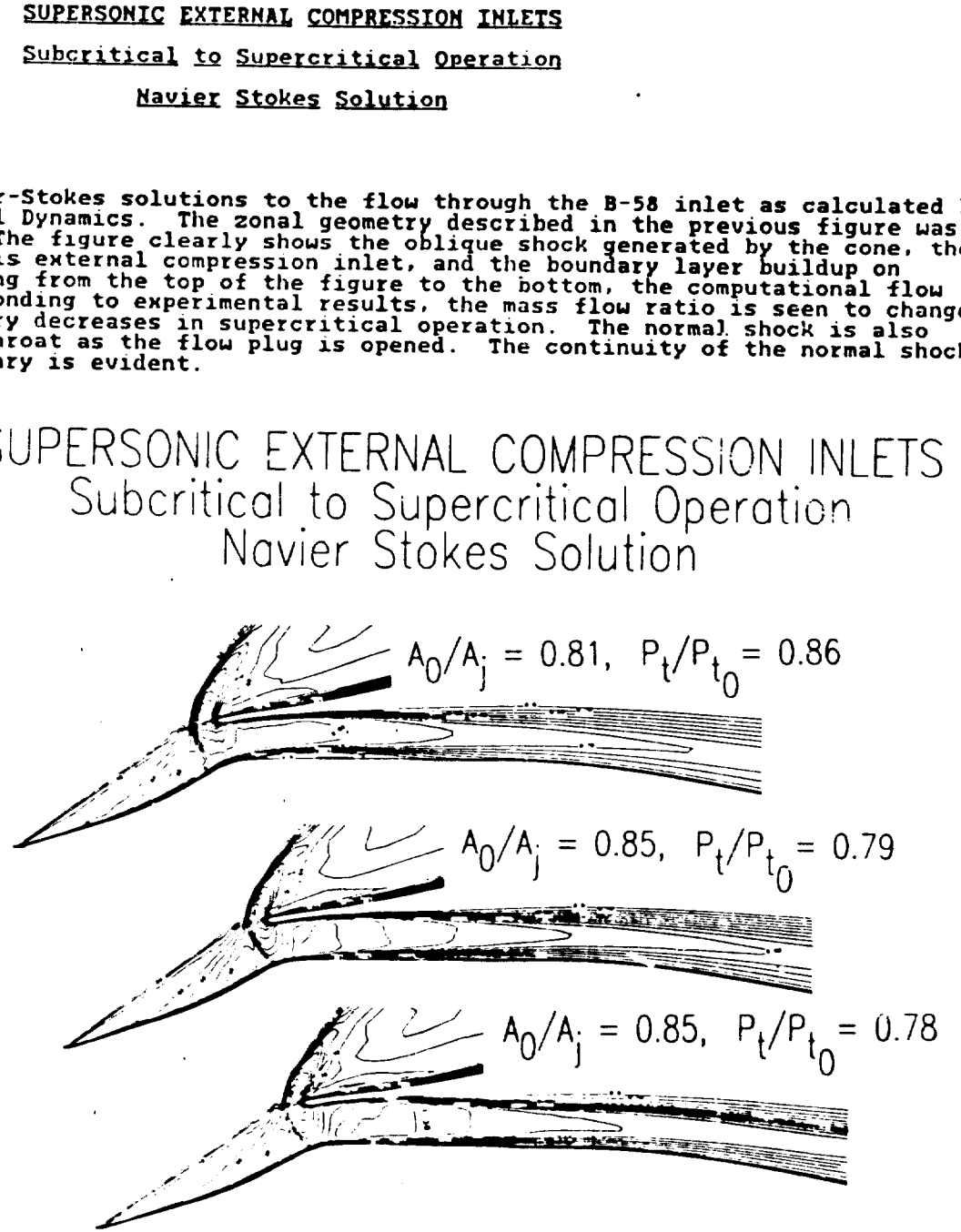

SUPERSONIC MIXED COMPRESSION INLETS

Fundamental Interactions

The character of the flow field within advanced supersonic inlets systems is three dimensional and highly complex. In the supersonic diffuser section upstream of the inlet throat the flow is characterized by strong three dimensional shock wave turbulent boundary layer interactions, both oblique and glancing. Large scale separation is surpressed by bleeding low energy boundary flow in the vicinity of the shock wave interactions. The placement of the bleed region relative to the shock boundary layer interaction has a significant effect on the state of the boundary layer downstream of the interaction zone. In general, the bleed amounts used for typical inlet configurations are large, often between 25 to 50 percent of the approach boundary layer mass flow. A performance penalty is incurred in maintaining a healthy non-separated boundary layer by bleeding. Because the bleed mass flow is not reinjected into the inlet, part of the capture mass flow is lost. To compensate for this loss in mass flow, a larger nacelle is needed which would increase friction drag and inlet weight. In addition, the bleed flow is usually vented overboard through bleed exits, a phenomenon which will cause a drag pentalty. Since supersonic inlets must operate over a large speed range, variable geometry features must be incorporated into the design. To the inlet designer, this will mean that the shock wave interaction will occur at different positions within the inlet with a concomitant shift in the bleed locations.

The terminal shock region is a very difficult problem which impacts upon the loss characteristics and stability characteristics of the inlet flow. In a practical mixed compression inlet, the requirement of shock structure stability determines to a large extent the normal shock loss in the inlet, itself a major contribution to the overall inlet losses. In essence by allowing some supersonic expansion after the geometric throat, i.e. supercritical operation, with subsequent shock down to subsonic flow via a normal shock, stability margin is obtained at the cost of the normal shock loss. If the normal shock were to occur very near the geometric throat where the local Mach number was unity, the resulting normal shock loss would be minimal but the inlet would be susceptable to unstarting. Having some supersonic reacceleration after the geometric throat places the normal shock downstream of the throat where a degree of stable upstream shock movement is possible without unstarting the inlet. This upstream shock movement could be unavoidable in practice, for instance, as the result of changing engine operating conditions or the result of changes in external flow. If the normal shock is pushed into the converging area ahead of the throat, by something like increased angle-of-attack or control error, it becomes unstable and will be abruptly expelled from the duct. This process is called inlet unstart, and the transient which will develop can be very violent and impart large unsymmetric forces to the aircraft.

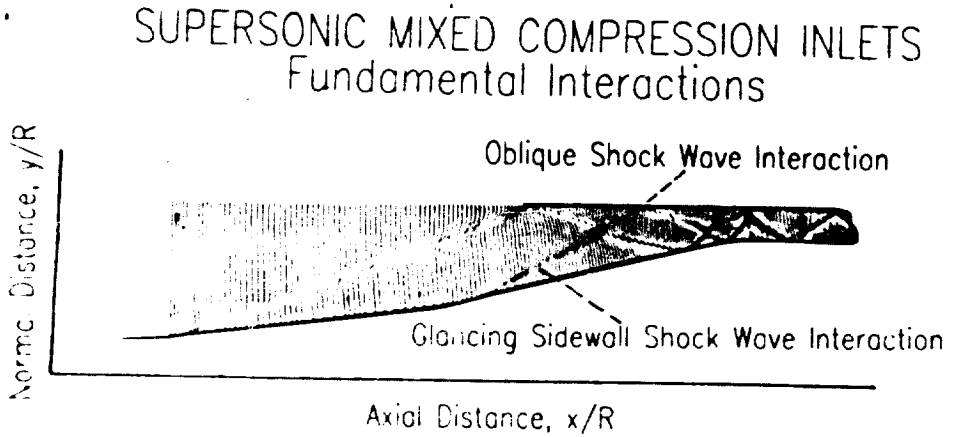

OBLIQUE SHOCK WAVE INTERACTION

Parabolic Navier Stokes Solution

Minf=3.88, Rey=5.0x10e6/ft.

In mixed compression inlets, oblique shocks are reflected from internal surfaces to compress the supersonic flow. A benchmark test case of the oblique shock wave turbulent boundary layer interaction has been experimentally studied by Rose (Ref. 26). The oblique shock was generated by a 10 degree cone placed in a blow down circular tunnel operating at Mach 3.88 and Reynolds number of 5.0E6 per foot. Benson and Anderson of the NASA Lewis Research Center , Ref (37), have studied this case using a supersonic PNS solver. In this calculation, the entire tunnel was modeled using a computation mesh of 89X450 (40,500 points) with approximately 30 points in the boundary layer. On the Lewis CRAY I computer, this benchmark test case took 0.9 minutes of CPU time. This figure presents comparison between the calculated and measured pitot pressure profiles through the interaction zone; the solid lines giving the results of the analysis and the circles giving the experimental results. The incident shock appears as a discontinuity in the experimental data, while shock smearing occurs over several grid points in the prediction. The analysis predicts well the development of the pitot profiles including the thinning of the boundary layer.

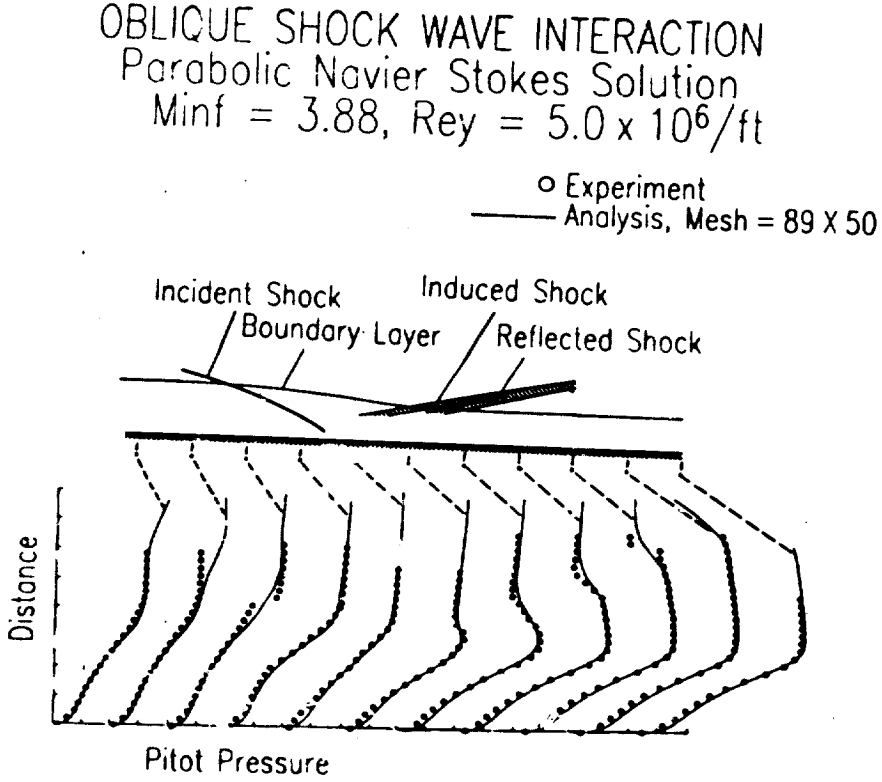

SUPERSONIC BOUNDARY LAYER BLEED CONTROL

Mach 2.5 Mixed Compression Inlet

Pitot Pressure Distribution

Centerbody Surface

One method of controlling the shock/boundary layer interaction within inlets is to bleed off the lowest portion of the boundary layer in the vicinity of shock reflections. The removed boundary layer flow is then ducted overboard with some drag penalty. Bleed is used on most currently operating supersonic aircraft and has been studied for many years both experimentally and computationally. This figure depicts the throat region of the NASA 40-60 axisymmetric mixed compression inlet; an inlet used to study various types, locations and amounts of bleed to maintain high inlet performance. The dashed lines in the upper portion of the figure show the inviscid shock reflections present in the inlet. The flow in the vicinity of the bleed zones was surveyed using traversing pitot probes, as shown in the figure. The flowfield was also caluculated using a Parabolized Navier-Stokes (PNS) code with bleed modeled. The bottom part of the figure shows a comparison of the computed results (solid lines) and experimental results (circles) for this inlet. The first two figures are located on either side of the reflected shock and indicate that the PNS code with bleed model is capable of accurately describing the flow in this region. With bleed, the boundary layer is thinned and the lower part of the boundary layer energized.

SUPERSONIC BOUNDARY LAYER BLEED CONTROL
Mach 2.5 Mixed Compression Inlet
Pitot Pressure Distribution
Centerbody Surface

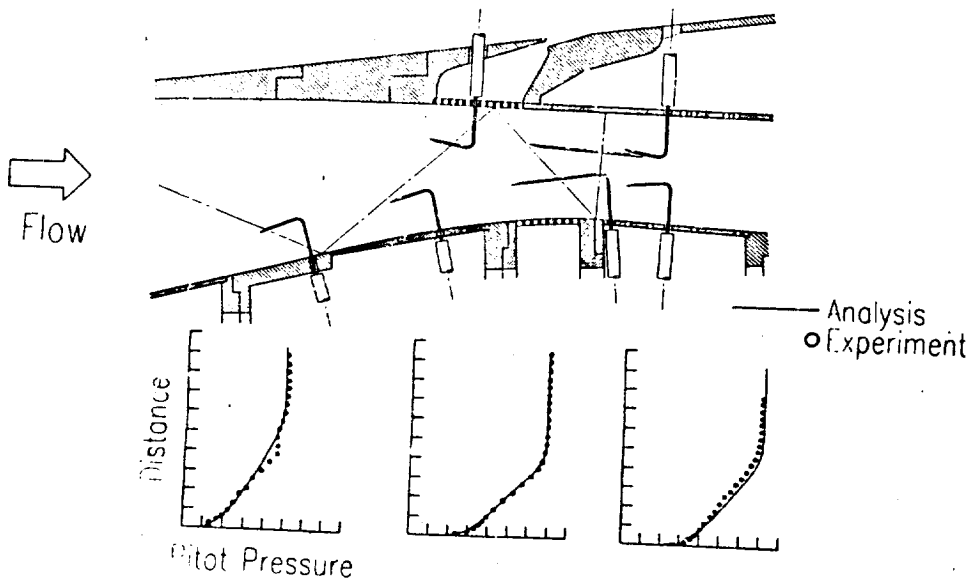

SUPERSONIC BOUNDARY LAYER BLEED CONTROL

Mach 2.5 Mixed Compression Inlet

Pitot Pressure Distribution

Cowl Surface

This figure is similar to the previous figure except that the comparison between experiment and analysis is made on the cowl surface. For this inlet, the bleed mass flow on the cowl surface was nearly ten times the amount on the centerbody. Still, the PNS analysis compares quite well with the experimental results and indicates a substantial thinning of the boundary layer through the bleed zone. When the computer analysis was attempted for this case with no bleed on the cowl surface, the analysis indicated massive separation of the boundary layer at this shock reflection. Bleeding the boundary layer was able to eliminate the separation, both experimentally and analytically.

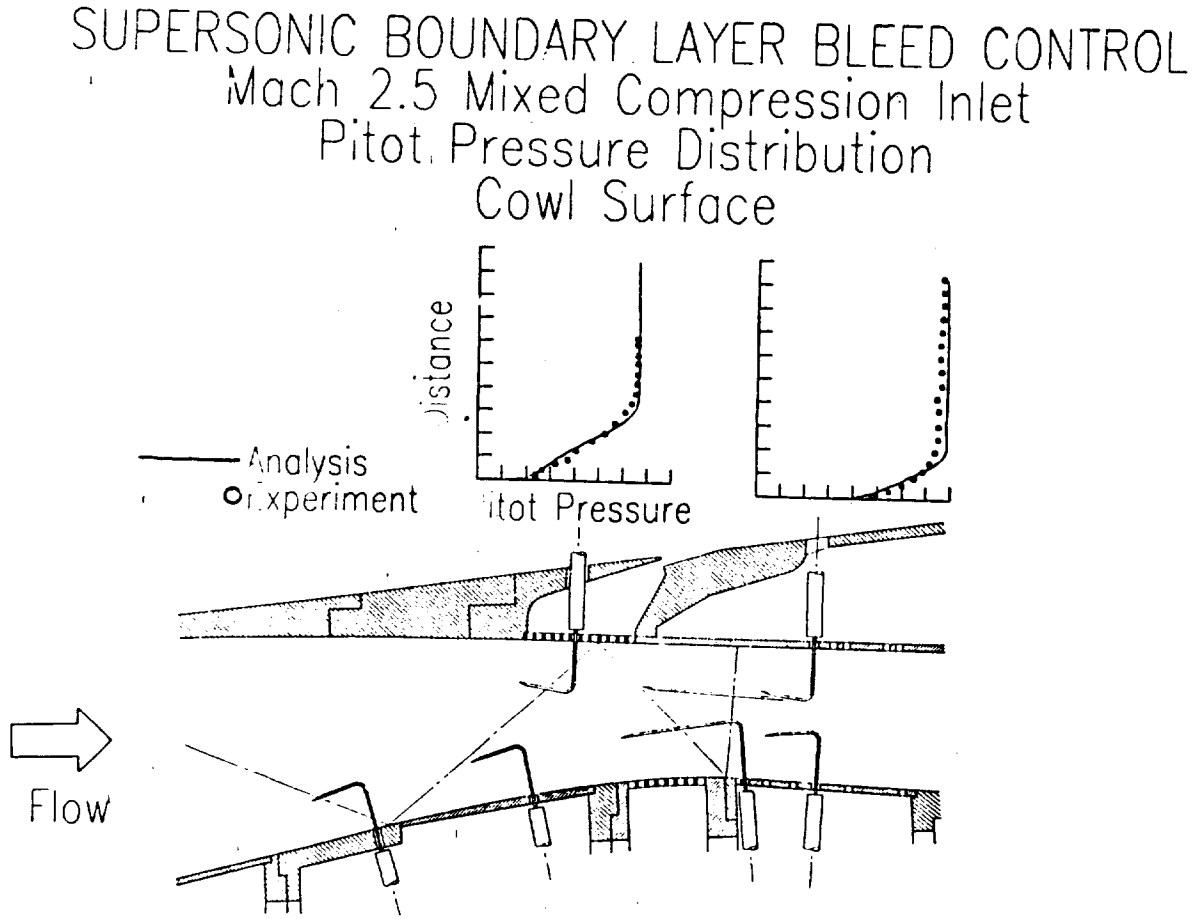

SUPERSONIC INLET BOUNDARY LAYER CONTROL SYSTEM

Bleed Hole Geometry and Relevant Parameters

Analysis and Experiment

The previous PNS calculations modelled the boundary layer control bleed as a distributed mass flow removal from the inlet. In practical application, boundary layer bleed is accomplished by mass removal through perforated plates. The size, shape and pattern of the descrete holes in this plate are important parameters in the operation of boundary layer bleed. For rows of discrete holes, the bleed geometry can vary in hole diameter, row spacing, hole spacing, aspect ratio, and hole angle. At present, computer models can not accurately model all of these parameters; but with more powerful computers, optimum bleed geometry or new methods of boundary layer control may be determined computationally.

SUPERSONIC INLET BOUNDARY LAYER CONTROL SYSTEM
Bleed Hole Geometry and Relevant Parmeters
Analysis and Experiment

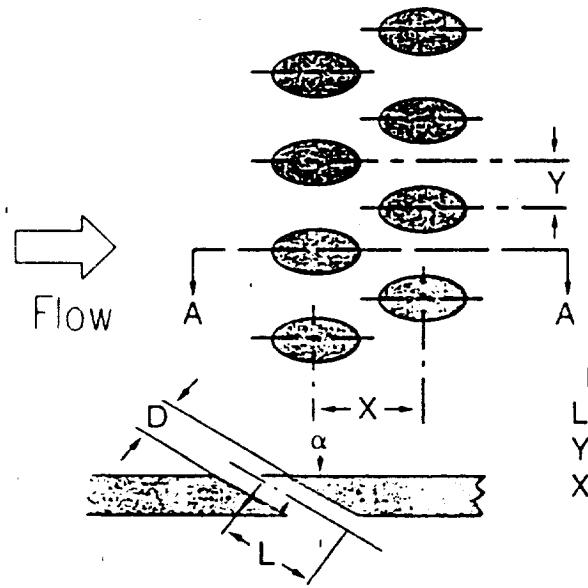

D Bleed Hole Diameter
L/D Bleed Hole Aspect Ratio
Y/D Bleed Hole Spacing
X/D Row Spacing
α Bleed Hole Angle

SUPERSONIC INLET BOUNDARY LAYER CONTROL SYSTEM

Computed Cowl Surface Shape (Hi) Factor

Boundary layer bleed systems within mixed compression inlets must operate over a range of flight conditions. For this reason, and to prevent recirculations within the bleed system, bleed is normally segmented in the inlet. One way of optimizing the location of the bleed segments is to calculate the shape factor of the boundary layer throughout the inlet at several operating conditions. Mapping the shape factor can indicate areas within the inlet where separation is likely to occur and where, therefore, bleed should be located. This figure show a map of shape factor (Hi) through a Mach 3.5 axisymmetric inlet as a function of free stream Mach number and inlet axial station. The regions selected for inlet bleed are indicated by the verticle bars. These calculations and the inlet design and tests were performed by Syberg and Hickcox of Boeing.

SUPERSONIC INLET BOUNDARY LAYER CONTROL SYSTEM
Computed Cowl Surface Shape Factor (Hi) Map

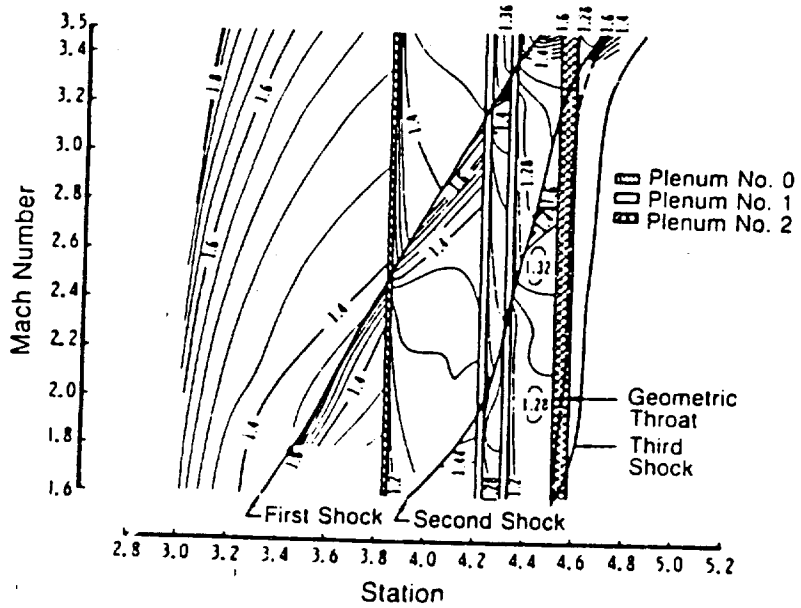

3D GLANCING SIDEWALL SHOCK WAVE INTERACTION

An importatnt interaction present in rectangular mixed compression inlets is the glancing shock boundary layer interaction. This interaction arises when the oblique shock wave formed by the wedge interacts with the wall boundary layer. Because of the skewing of the incident shock wave across the boundary layer on the wall, a strong transverse static pressure gradient is established which generates strong cross flows. A schematic diagram depicting the analytical and experimental test configuration used to study the glancing sidewall turbulent boundary layer interaction is shown in this figure. The nominal Mach number upsream of the wedge was 2.84, the tunnel total pressure was set at 88.9 psia and the tunnel free stream total temperature was 445.0 degree Rankine. Two computational mesh systems were used to study the glancing sidewall boundary layer interaction. a coarse grid composed of 40X40X100 (160,000) points and a medium grid with 40X60X90 (216,000) points. On the Lewis CRAY I high speed computer, these calculations were accomplished using 6.0 and 9.6 minutes of CPU time respectively. Shown in subsequent figures is a comparison of the computed and measured yaw angle distribution through the wall boundary layer. The yaw angle is defined as the ratio of the velocity in the YG-direction which is parallel to the tunnel sidewall, divided by the velocity in the X-direction. This is a particularly difficult parameter to calculate since it represents the ratio of two velocities which approach zero as the wall is approached. It is apparent that very good agreement was obtained using the analysis to model this important interaction. A detailed study of the effects of wall functions and grid resolution was performed by Anderson and Benson, Ref (36), using a PNS solver. They concluded that insufficient mesh resolution of the near wall region caused discrepancies to appear in the calculation of the velocity field.

GLANCING SIDEWALL SHOCK INTERACTION
Test Geometry

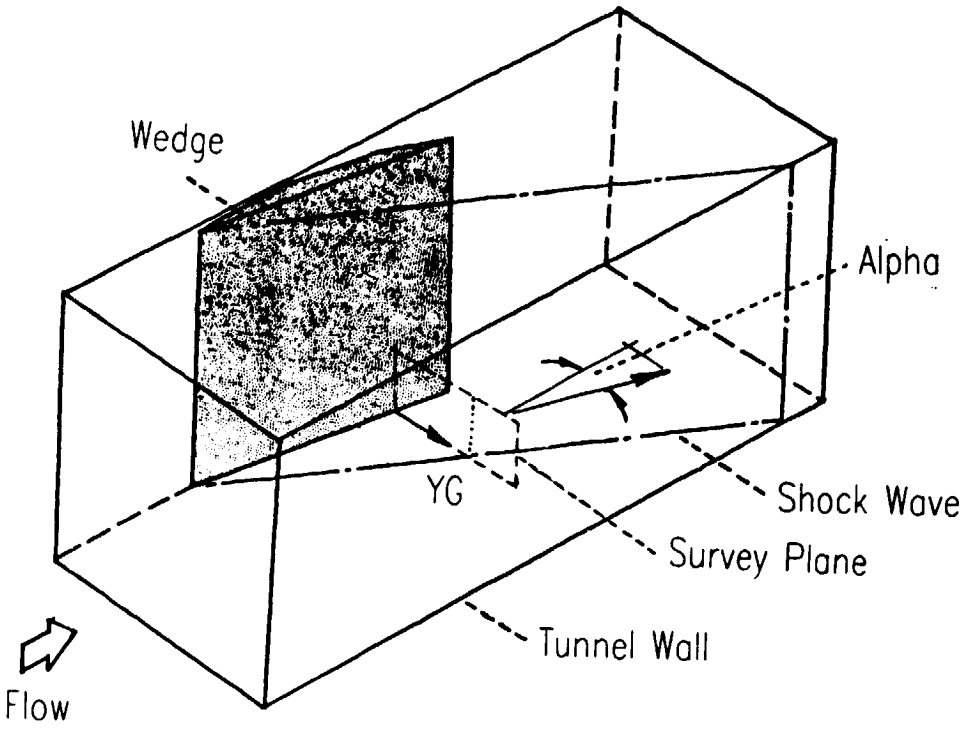

GLANCING SIDEWALL SHOCK INTERACTION
Minf = 2.94, Wedge Angle = 10.0, Rey = 1.28×10^6
Yaw Angle Distribution

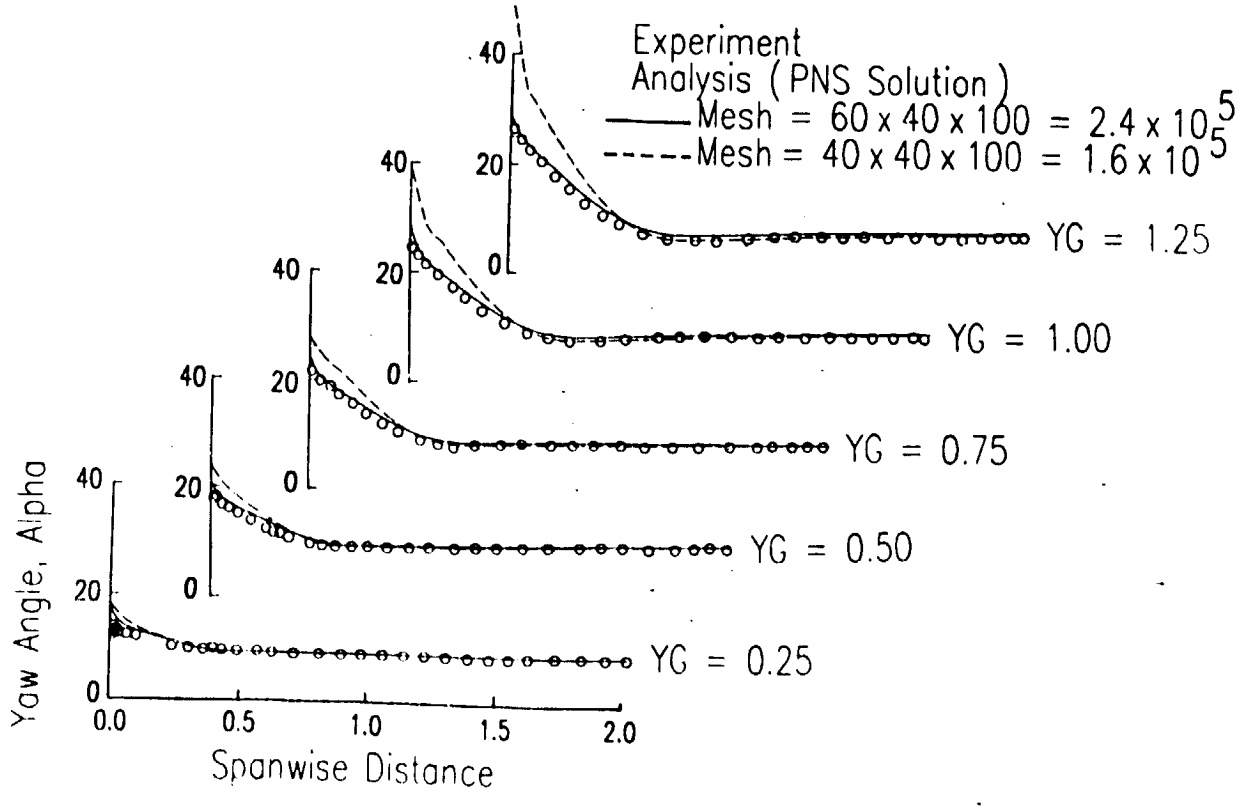

GLANCING SIDEWALL SHOCK INTERACTION
Minf = 2.94, Wedge Angle = 10.0, Rey = 1.28×10^6
Yaw Angle Distribution

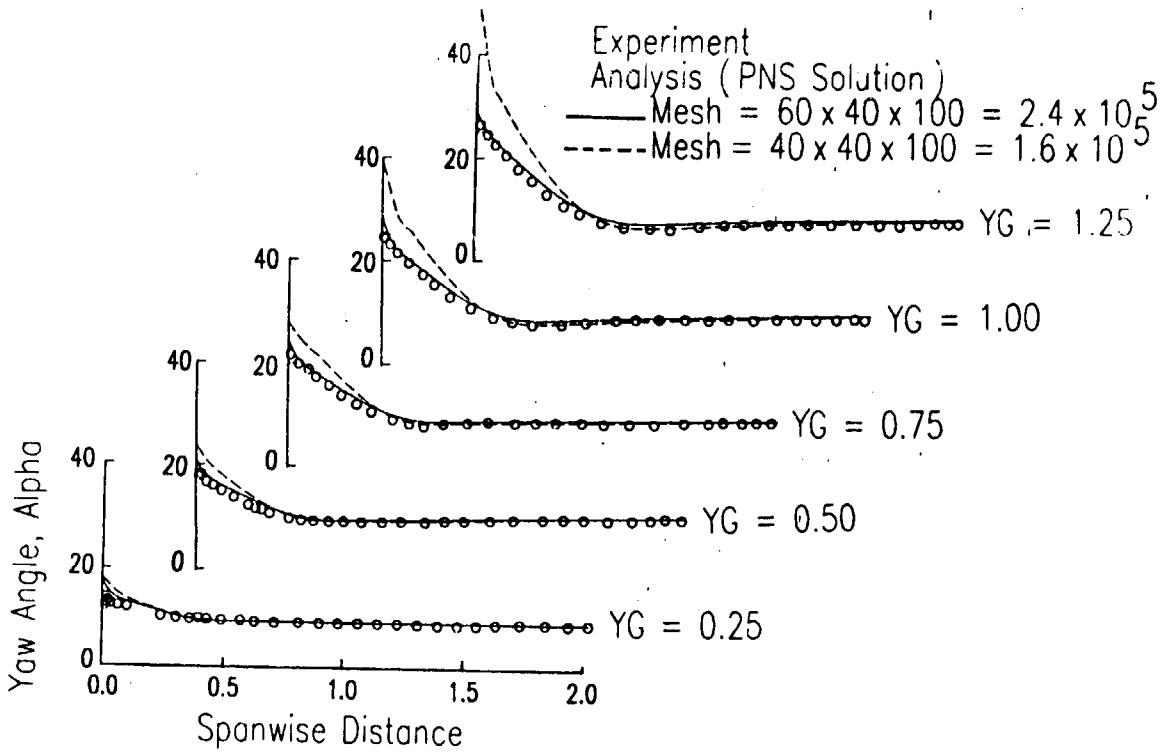

GLANCING SIDEWALL SHOCK INTERACTION
Minf = 2.94, Wedge Angle = 10.0, Rey = 1.28×10^6
Yaw Angle Distribution

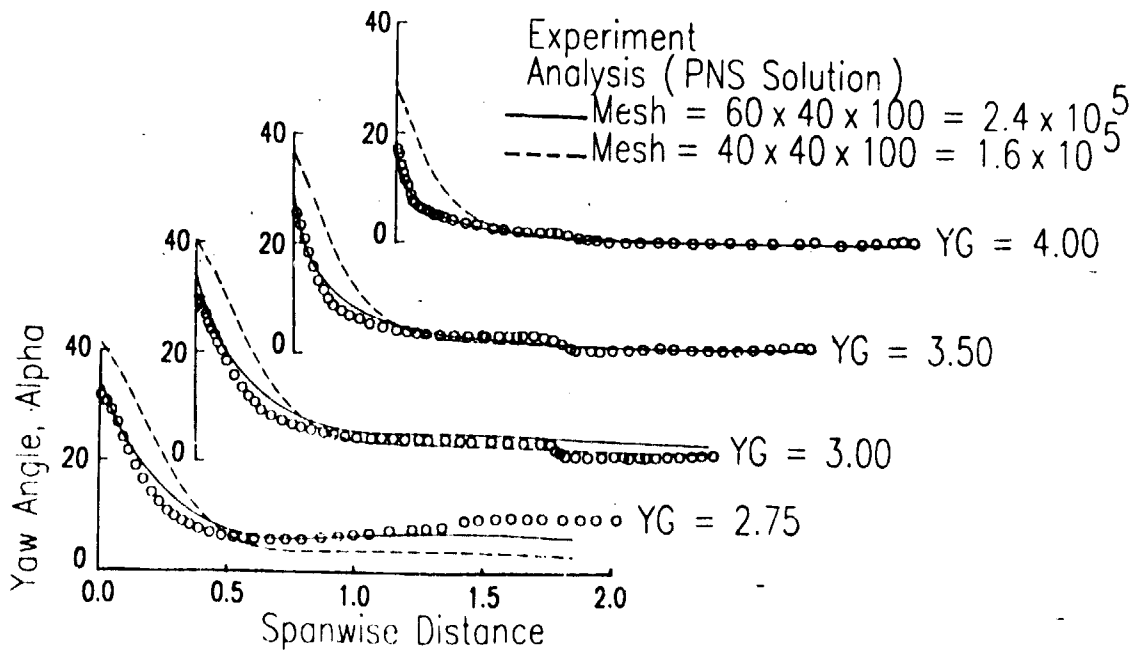

GLANCING SIDEWALL SHOCK INTERACTION

Velocity Vectors

A detailed picture of the velocity field in the tunnel sidewall region is shown in the next two figures. Along the wall, the flow is turned at nearly the wave angle instead of the wedge angle, and flow downstream of the shock proceeds in a conical fashion. In the vicinity of the tunnel sidewall, a very strong vortex is established which elongates and increases in strength in the downstream direction. This causes very low energy flow to accumulate in the corner region with resulting low wall shear stress in this region. This probably accounts for the very high heating rates measured by Oskam, Vas and Bogdonoff (Refs. 27-29). The increased strength of the sidewall vortex is also suggested by the experimental data, since the maximum yaw angle increases in the downstream direction. The oveturning that occurs in the sidewall boundary layer results from an imposition of the main stream static pressure gradient upon the low momentum near wall viscous flow. This overturning results in low energy fluid being drawn in towards the tunnel sidewall in the lower ramp region. In the outer ramp region, the flow rolls over to form the sidewall vortex. As the flow develops in the downstream direction, the sidewall vortex losses its identity and the surface velocity vectors tend to align themselves with the shock angle.

The global features of the glancing side interaction that emerge from this study can be viewed in terms of two separate flow regions, namely a large outer region of inviscid high energy flow which follows the inviscid stream lines, and a smaller inner region near the wall composed of low energy fluid which migrates along the shock wave. The low energy flow will eventually accumulate in the corner region of the tunnel ceiling causing severe problems. This flow is called the glancing sidewall/corner shock wave turbulent boundary layer interaction and will be discussed later in this paper.

GLANCING SIDEWALL SHOCK INTERACTION
Near Surface Velocity Vectors

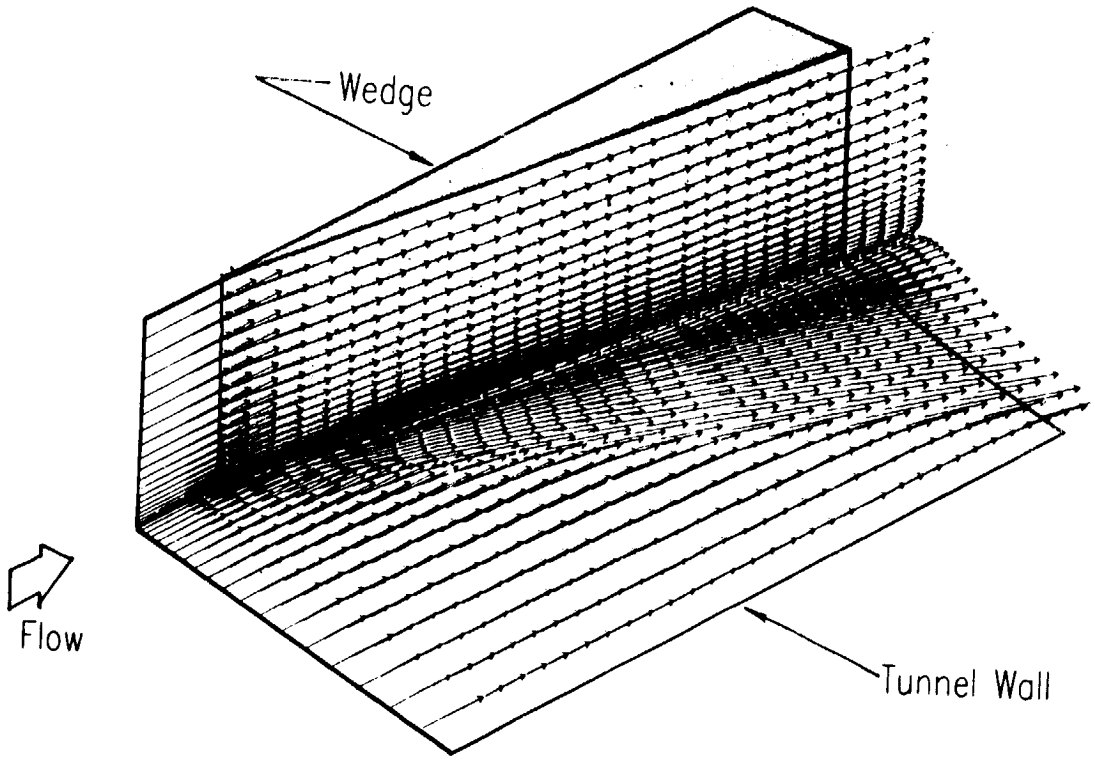

GLANCING SIDEWALL SHOCK WAVE INTERACTION
Secondary Velocity Vectors

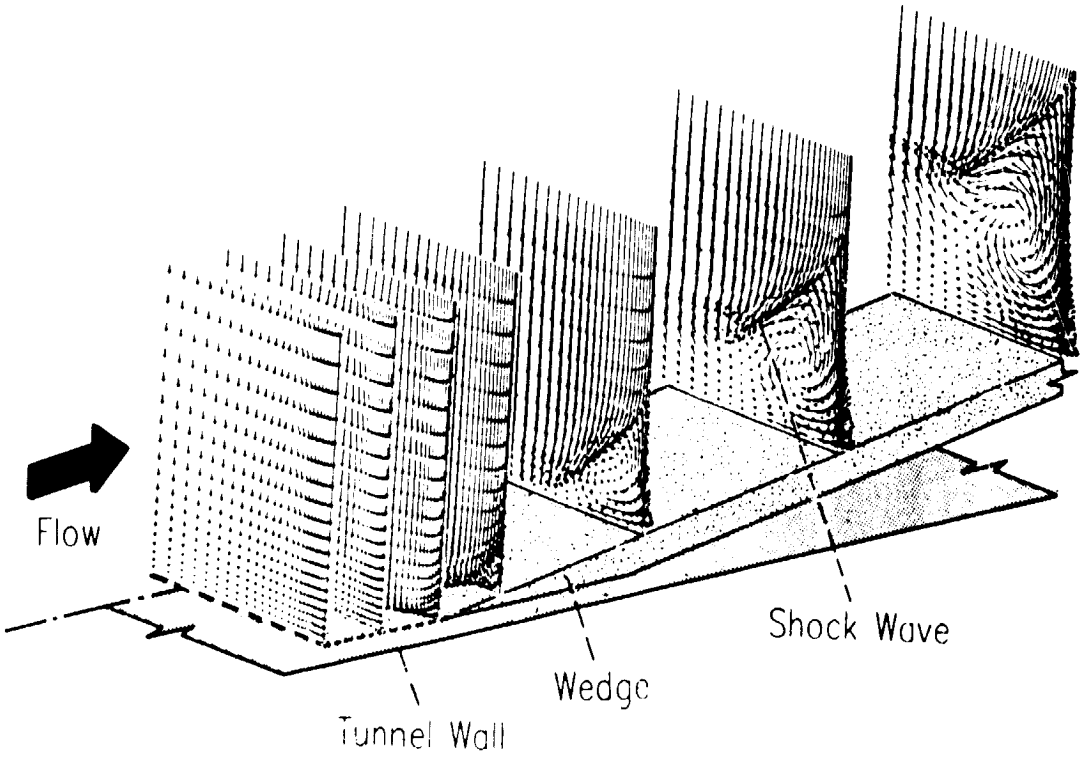

GLANCING SIDEWALL SHOCK INTERACTION

Experimental Oil Film Patterns

To study the effects of the glancing shock sidewall boundary layer interaction on inlet performance, a series of experiments were run in the NASA Lewis 1X1 supersonic wind tunnel. The interaction was studied at various Mach numbers, shock generator angles, and with boundary layer control provided by sidewall bleed. This figure shows one typical result at Mach 3.0 with a ten degree wedge angle. The wedge is located at the top, the shock glancing across the tunnel wall boundary layer and reflecting from the bottom surface. This figure shows surface oil flows in the vicinity of the interaction. One can see that the sidewall flow has been turned much greater than ten degrees, that the entire low energy region of the sidewall has been swept into the corner formed by the sidewall and the tunnel floor. There is a large separated region in this corner and an additional separation region located along the centerline of the tunnel where the shock reflects. Flow downstream of the shock location on the sidewall is conical, which is consistant with the results of Bogdonoff.

GLANCING SIDEWALL SHOCK INTERACTION
Experimental Oil Film Patterns

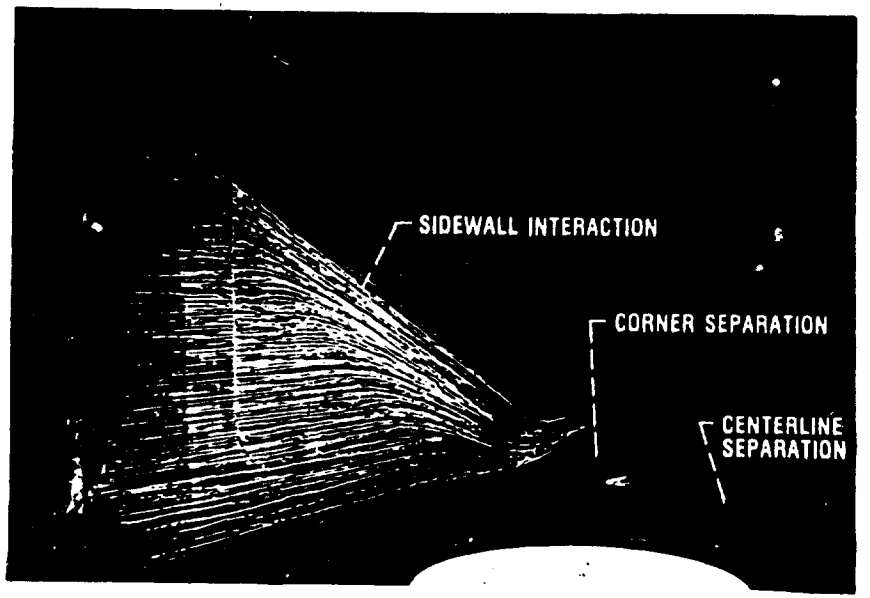

GLANCING SIDEWALL SHOCK INTERACTION

Analytical Oil Film Patterns

The flow problem described in the previous figure has been calculated using a supersonic PNS comoputer code. The numerical oil flow results are presented in this figure for comparison with the previous experimental results. The analysis correctly predicts the sweeping of the sidewall oil into the corner formed by the sidewall and the tunnel floor. In this corner the analysis also indicates a flow separation. The separation along the centerline is indicated in the computational results, but the full upstream influence of this interaction is not correctly modelled because a single sweep PNS analysis has been used. The code also indicates that the flow along the sidewall downstream of the shock is conical in nature.

GLANCING SIDEWALL SHOCK INTERACTION
Analytical Oil Film Patterns

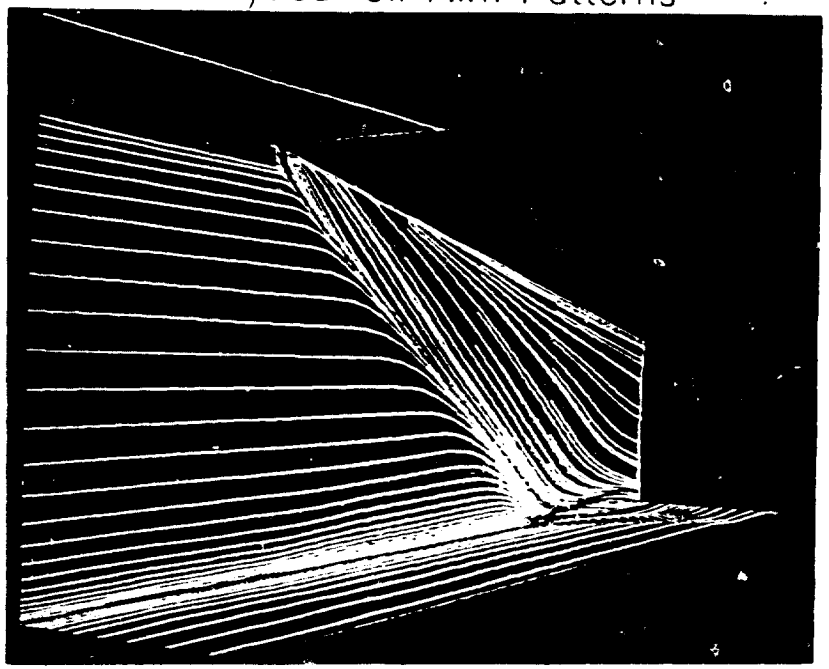

GLANCING SIDEWALL SHOCK INTERACTION
Analytical Oil Film Patterns

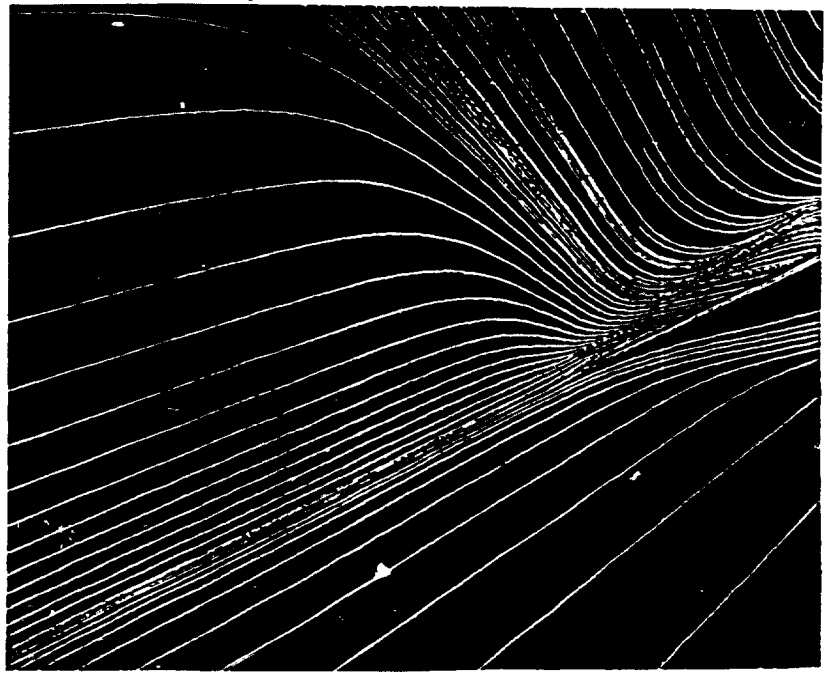

GLANCING SIDEWALL SHOCK INTERACTION

Corner and Centerline Separation Regions

Experimental Oil Flow Patterns

This is a detailed photograph of the corner and centerline separation present in the glancing shock studies in the NASA Lewis 1X1 supersonic tunnel. The corner separation, at the top, has been caused by an accumulation of low energy flow in the corner due to the glancing shock/sidewall boundary layer interaction. When this low energy flow is subjected to the adverse streamwise pressure gradient of the shock reflection, the flow separates. Along the centerline, at the bottom, separation occurs because of the oblique shock reflection. The pressure rise through the reflection has been calculated with the Lewis PNS code and found to exceed the inviscid pressure rise because of the three-dimensional nature of the flow through the corner. Along the centerline, the oil flow indicates that a large reverse flow region is present.

GLANCING SIDEWALL SHOCK INTERACTION
Corner and Centerline Separation Regions
Experimental Oil Flow Patterns

MACH 5.0 HYPERSONIC INLET

CFD Validation Configuration

Fundamental Interactions

The Mach 5.0 mixed compression inlet was designed under contract to NASA Langley and is to be tested in the NASA Lewis 10X10 wind tunnel. This inlet was designed using a method of characteristics analysis with the surfaces corrected for boundary layer displacement effects. In most supersonic inlet designs the correction for boundary layer displacement is quite small, but in hypersonic inlet designs the boundary layer displacement can become very large. A schematic drawing of the mixed compression inlet is shown in this figure. The inlet has rectangular cross-section, a pre-compression ramp and three compression ramps external to the cowl. The aircraft flying at angle of attack generates a shock wave at the leading edge of the pre-compression plate. This shock and the shocks from the ramps are designed to fall just outside the cowl lip at the design Mach number, as shown by the dashed lines. The cowl lip generates a shock which is cancelled at the ramp shoulder and the cowl is contoured to further compress the flow internally. A swept sideplate runs from the leading edge of the pre-compression plate to the leading edge of the cowl to minimize the drag generated by compressed flow spilling over the sides of the inlet. Similar swept sideplates have been used on rectangular inlets for the F-15, F-14, B-1A and XB-70, although all of these aircraft were designed for the Mach 2.0 to 3.0 speed range.

A PNS analysis was first performed two-dimensionally to verify the inlet design condition of shock cancellation near the shoulder. The free stream Mach number was 5.0, angle of attack was 9.0 degrees and Reynolds number per foot was 2500000. The results of this calculation are shown in the bottom figure which shows Mach number profiles at various locations through the inlet. The location of shock waves are noted by the abrupt change in profile. This figure indicates that, in spite of the large displacement correction, the shock from the cowl has been cancelled at shoulder and that this is a good two-dimensional design for the Mach 5.0 condition. The figure also shows the extremely thick boundary layer that forms on the ramp surface at Mach 5.0; approximately one third of the flow into the inlet is boundary layer. Near the throat of the inlet, the boundary layers from the ramp and cowl surface have merged. Predictions of static pressure rise and total pressure loss through the compression system agree well with method of characteristic results corrected for boundary layer effects.

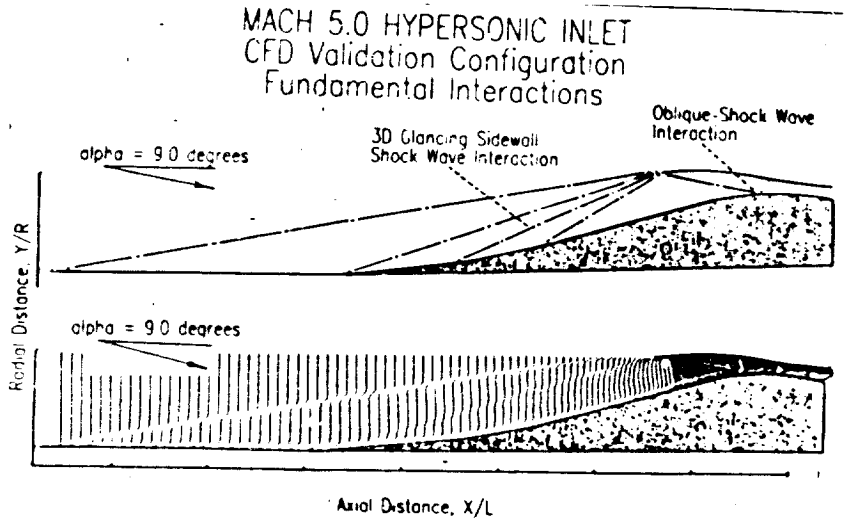

MACH 5.0 HYPERSONIC INLET

Mach Number and Secondary Velocity

The Mach 5.0 inlet described in the previous figure has been analyzed three-dimensionally using the PNS analysis program. The free stream conditions for the three-dimensional case were the same as those in the two-dimensional inlet case. Because the shock generated by the pre-compression ramp lies just along the edge of the swept sideplate, a zero derivitive boundary condition has been used in the flowfield along the side. No slip boundary conditions have been used along the solid surface of the sideplate. The computations were performed on an 80X60 cross-sectional grid, which corresponds to the levels of grid resolution required for accurate modelling of the glancing shock boundary layer interaction (GSBLI). The inviscid Mach number aft of the pre-compression shock is on the order of 4.0, which is very close to our established data base for the GSBLI.

The results from the three-dimensional calculation are presented in a series of figures . At the top of each figure is a schematic of the inlet, with the location of the cross-sectional plane given by a vertical line and a prescribed distance from the inlet leading edge. The bottom of the figure shows the flowfield in a cross-section of the inlet; the ramp surface is at the bottom, the cowl surface at the top, and sideplates are on both sides. Because of flow symmetry, only half of the inlet was calculated. The left side of the figure shows Mach number contours, while the right side show secondary velocity within the cross-sectional plane. The figures proceed from a location just upstream of the cowl leading edge to a location near the throat. On the solid surface of the ramp, cowl and sideplate, one will note the development and growth of the boundary layer by a concentration of Mach contours near these surfaces. Shock waves are noted by a concentration of Mach contours away from the solid surfaces. They can also be detected by an abrupt change in the secondary velocity vectors. In this calculation, the compression shocks and the Mach contours are parallel to the ramp and cowl surfaces.

Near the cowl lip, the flow field appears as shown in the first figure. The secondary velocity vectors show extremely strong flow along the sideplate, while the Mach number contours show the sideplate boundary layer to be highly distorted. The boundary layer has been thickened in the vicinity of the shock waves and thinned in the corner formed by the ramp and sideplate by the GSBLI from each compression ramp. The secondary velocity vectors also show flow being drawn along the ramp surface into this corner. The boundary layer along the ramp surface is quite thick and corresponds to the thickness predicted in the two-dimensional calculations. The strong secondary flows induced by the multiple GSBLI persist even though the shock waves have left the flow domain over the cowl. The flowfield from the inlet leading edge to the cowl lip has been shaped by the thick boundary layer that grows on the ramp and sideplate and the multiple GSBLI that occur on the sideplate due to the compression ramps. The flow is highly three-dimensional at the cowl lip with low energy boundary layer flow being swept up along the sideplate.

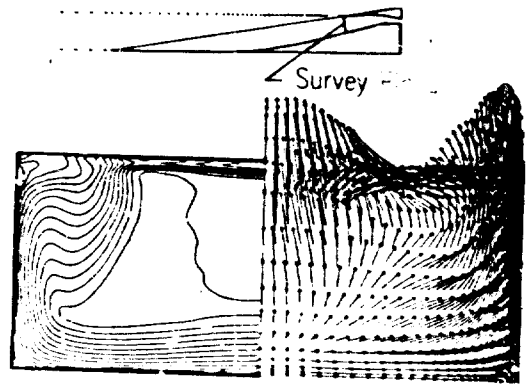

MACH 5.0 HYPERSONIC INLET

Mach Number and Secondary Velocity

Continued

As the flow enters the cowl, the following figures show that a shock wave is generated by the cowl lip. This shock, indicated by the horizontal lines in the Mach contours, moves down through the flow field as shown. The strong secondary flow moving up the sideplate encounters the internal cowl surface and the secondary velocity vectors indicate that this flow turns through the corner formed by the cowl and sideplate. Two things happen as the secondary flow turns this corner; first, the secondary flow rolls up into a vortex, and second, the low energy flow is concentrated in the corner. The internal surface of the cowl has been shaped to further compress the flow. As the low energy flow in the corner is subjected to the adverse pressure gradient created by this turning, a large separation occurs in the corner.

The inlet and the calulation has provisions for boundary layer control bleed on the ramp, cowl and internal sideplates. The amounts of bleed necessary to maintain inlet operation has been estimated from two-dimensional calculations. Applying this level of bleed allows the calculations to proceed to the inlet throat, but does not eliminate the distortion and separation created by the GSBLI.

The PNS analysis employs a FLARE approximation in the vicinity of small separations. In this model the negative streamwise convective velocity is reset to a small positive velocity. All details of the flow within the recirculating region are lost, but often the marching analysis can continue until the flow re-attaches. In the case of the Mach 5.0 inlet however, the magnitude of the separation was so great that the analysis could not be marched further. The existence of a large separation in the corner of the inlet would probably trigger an inlet unstart at these conditions. Even if the inlet remained started, the existence of the vortex near the sidewall and the distortion of the sideplate boundary layer as shown in these figures would pose major problems for the propulsion system.

MACH 5.0 HYPERSONIC INLET
Mach Number and Secondary Velocity

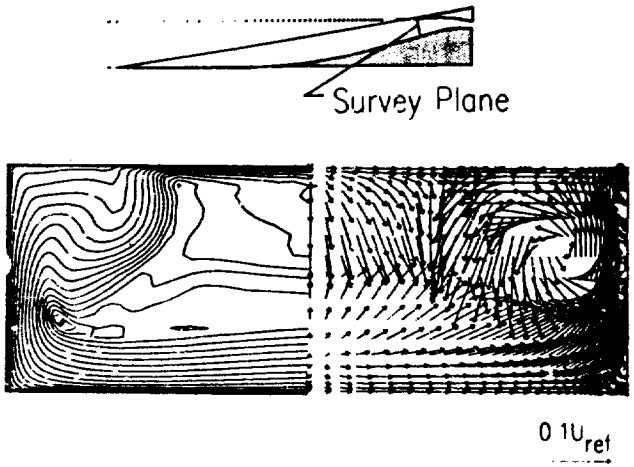

MACH 5.0 HYPERSONIC INLET
Mach Number and Secondary Velocity

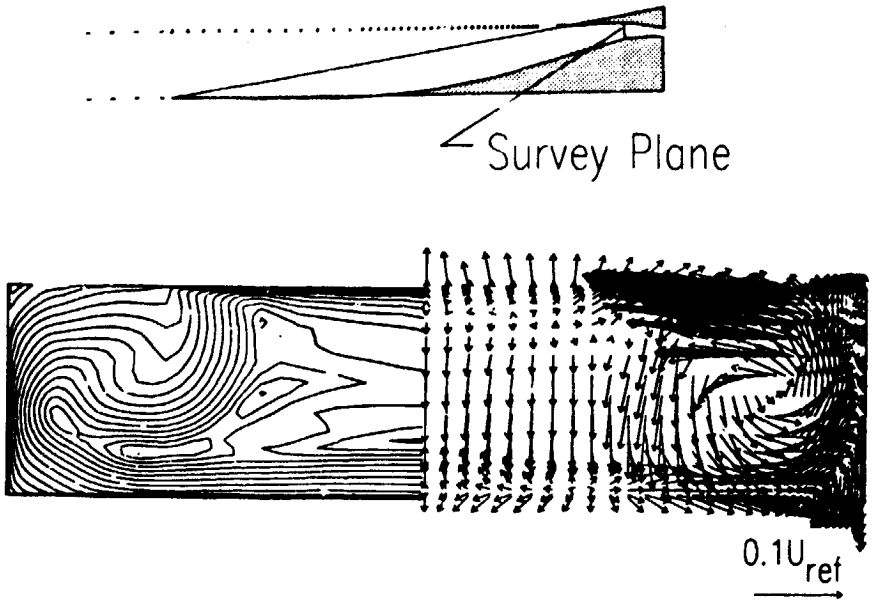

MACH 5.0 HYPERSONIC INLET
Mach Number and Secondary Velocity

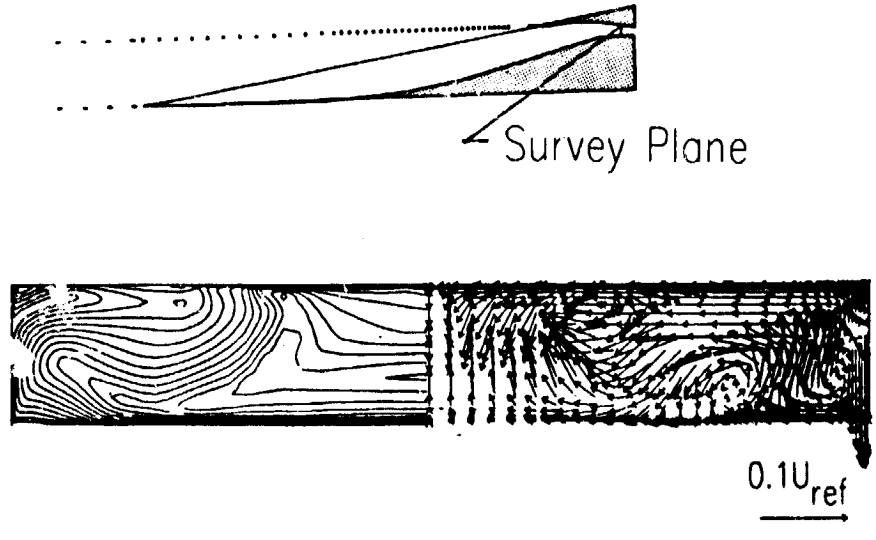

MACH 5.0 HYPERSONIC INLET

Cowl Surface Shear Stress

This figure depicts the computed shear stress on the internal cowl surface of the Mach 5.0 mixed compression inlet. The shear has been color coded, with red being the highest and purple the lowest levels of shear stress. The cowl of the inlet is at the top, the ramp surface at the bottom and the sidewalls on either side. One can see that in the corner formed by the cowl and sidewall a large region of low shear exists. This corresponds to the low energy and separated flow regions seen in the previous figures. The high shear regions along the centerline near the back of the inlet are produced by the reflected shock from the ramp surface and the bleed zones to control the shock reflection. The three-dimensional nature the flow in this inlet is clearly demonstrated in this figure.

MACH 5.0 HYPERSONIC INLET
Cowl Surface Shear Stress

MACH 5.0 HYPERSONIC INLET

Centerbody Surface Shear Stress

This figure, like the previous figure, shows color coded shear stress in the internal portion of the Mach 5.0 inlet. The cowl has been removed in this figure to show the ramp surface and sidewall conditions from the cowl lip station through the throat of the inlet. At the top of the sidewall, one notices a large low shear region corresponding to the low energy and separated flow in the corner formed by the sidewall and cowl. The low energy region remains thoughout the inlet despite shock reflections and boundary layer bleed which can often remove low energy flow. Along the corner formed by the side wall and ramp, other separated regions occur in the vicinity of shock reflections. This phenomenon was noted earlier in the benchmark studies of glancing shock/sidewall boundary layer interactions. As with the previous figure, high shear regions exist along the ramp in the vicinity of shock reflections and where boundary layer control bleed is used. The three-dimensional character of the shear distributuion is the result of glancing shock/boundary layer interactions between the reflecting compression shocks and the thick boundary layers on the sidewall.

MACH 5.0 HYPERSONIC INLET
Ramp Surface Shear Stress

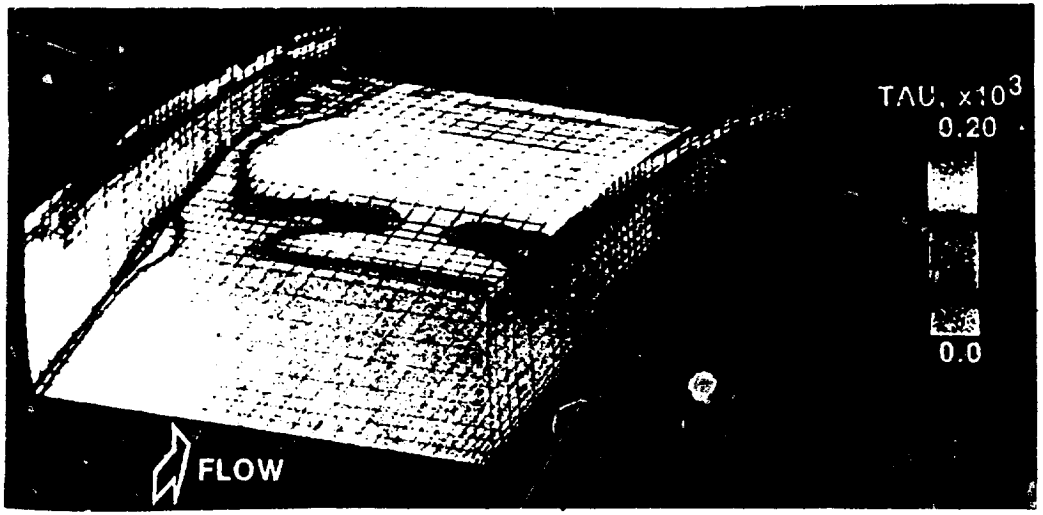

INTERNAL/EXTERNAL EMBEDDED BODY METHODS

Sideplate Spillage and Additive Drag

The calculations of the Mach 5.0 inlet have demonstrated the importance of three-dimensional effects in high speed inlets. To minimize these effects, the inlet designer is faced with a difficult problem. The origin of the three dimensional problems is the interaction of the compression shock system with thick boundary layers that build up on the sidewall. The simplest solution would be to eliminate the sidewalls upstream of the cowl. While this would minimize the inlets distortion problems, it would produce an inlet with excessive side spillage drag; flow pressurized by the compression shocks would be blown aound the side of the inlet. A compromise solution would be to notch the side plate to allow some spillage of the low energy flow swept by the compression shocks. The rest of the low energy flow may be controlled with boundary layer bleed, either along the sidewall or concentrated in the corners of the inlet. To aid in this trade study of inlet spillage drag versus bleed drag and distortion, the computational domain of the PNS computer code is being extended to include not only the capture streamtube, but also the flow around the inlet.

INTERNAL / EXERNAL EMBEDDED BODY METHODS
Sideplate Spillage and Addative Drag

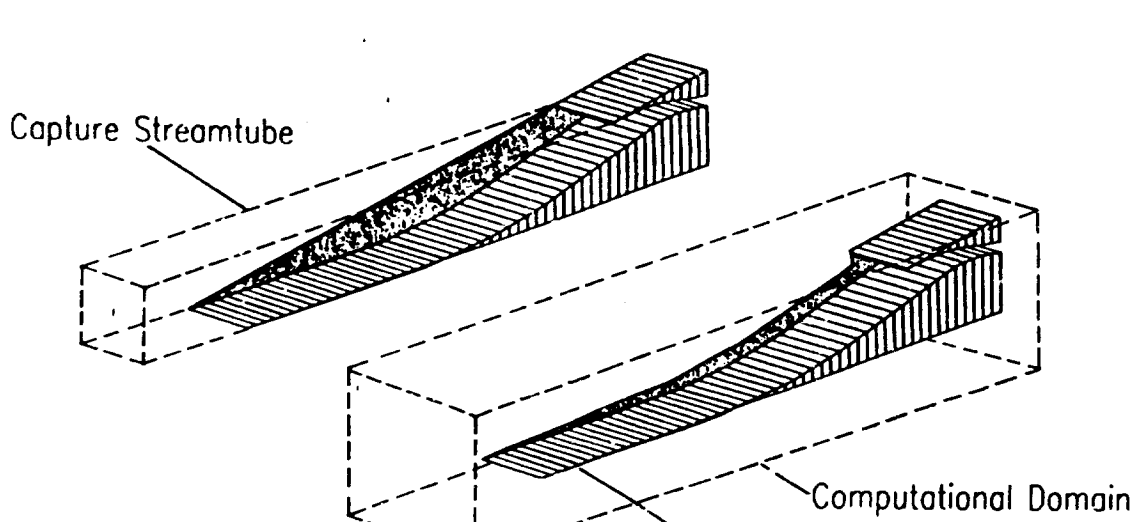

UNSTEADY INLET FLOW FIELD ANALYSIS

Inlet Unstart, Restart and Buzz

The mixed compression inlet is designed to provide high inlet recovery and low drag by keeping the terminal normal shock within the inlet duct. Under some conditions, however, the terminal shock may be perturbed and be disgorged from the inlet; the inlet is then said to be "unstarted". The inlet then performs in an external compression mode, with the corresponding decrease in recovery and increase in drag. The transition from started to unstarted can occur in a fraction of a second with catastrophic results for the inlet, engine and aircraft. While the inlet is in external compression mode, another phenomenon know as inlet buzz may occur. This is a periodic, high frequency movement of the terminal shock along the compression surface. Such an occurance can result in unsteady distortion to the engine, control problems for the inlet and aircraft and fatigue problems for the inlet.

To determine a proposed inlet's susceptibility to inlet unstart and buzz, several different analytical techniques have been used. The earliest techniques employed lump parameter Helmholtz resonator analogies to determine natural frequencies of the inlet ducts. To study the flow field effects, characteristic solutions were also developed. More sophisticated one-dimensional wave equation studies have also been used to assess an inlet's unsteady characteristics. Large perturbation analysis of the momentum and continuity equations have allowed more detailed studies of the inlet with respect to changes in pressure and mass flow. The latest computational efforts have centered on time accurate solutions to the Navier-Stokes equations in two and three dimensions. Much future work will involve time accurate studies of inlet flow fields.

UNSTEADY SUPERSONIC FLOW FIELD ANALYSES
Inlet Unstart, Restart and Buzz

(1) Helmholtz Resonator Analogies

(2) Characteristics Solutions

(3) Analysis of Wave Amplification

(4) Large Perturbation Flow Field Analysis

(5) Time Accurate Navier Stokes Analysis

MACH 2.5 MIXED COMPRESSION SUPERSONIC INLET

Unstart/Restart Transients

The Mach 2.5 40-60 mixed compression inlet has been studied experimentally and computationally to determine its unstart and restart capabilities. In the experiment a disturbance door was closed to create a back pressure disturbance. This disturbance caused the inlet to unstart, and certain mechanical features in the inlet, including a control bypass door and the postion of the centerbody were changed automatically to restart the inlet. The large perturbation analysis modelled the mechanical controls and calculated pressures at specific locations in the inlet where experimental probes were located. The figure shows a comparison of the experiment (solid lines) and the analysis (dashed lines). In general the comparison is quite good; the analysis is able to model the initial unstart transient both in magnitude and in duration. The experiment shows a more gradual return to started conditions than does the analysis, but the analysis is inviscid and one-dimensional which would tend to produce sharper transients.

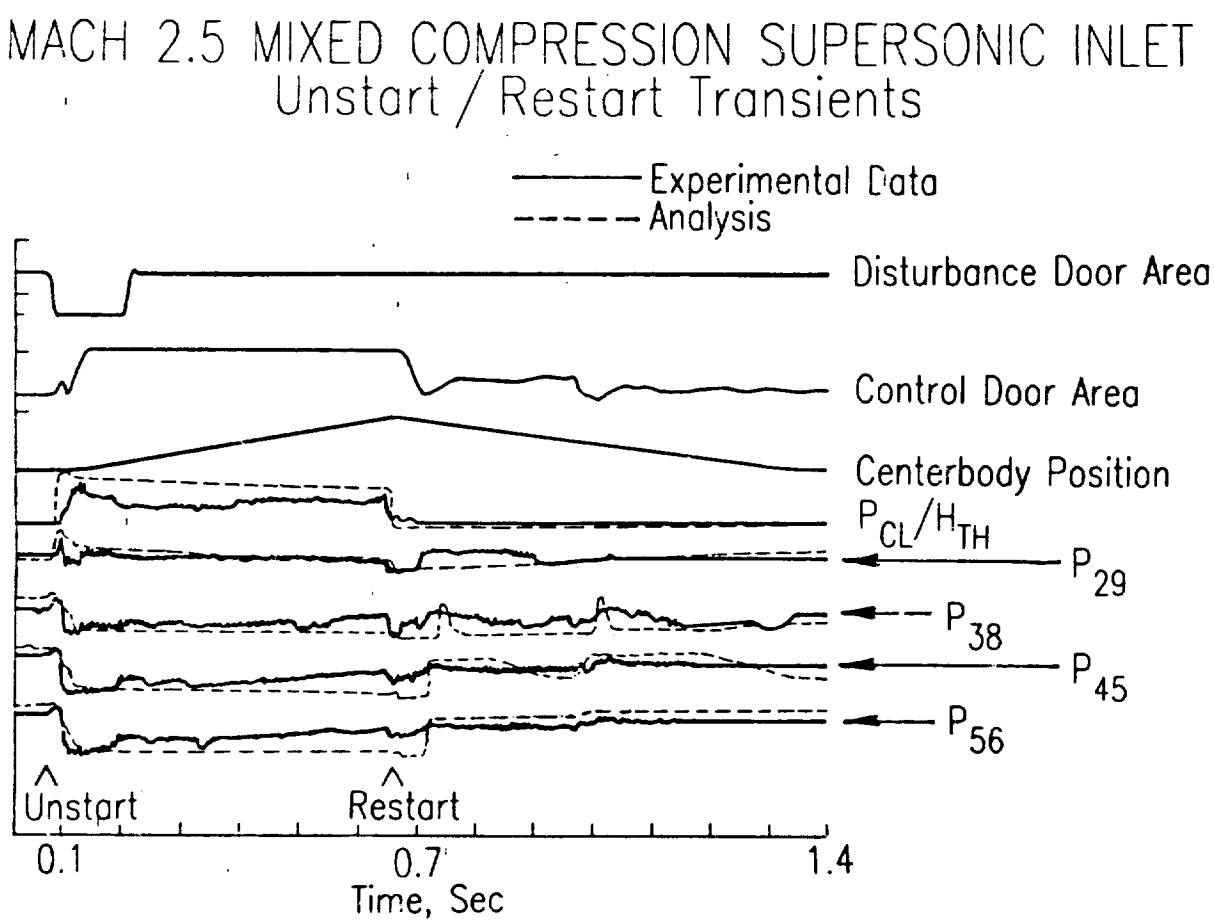

MACH 2.5 MIXEED COMPRESSION SUPERSONIC INLET

Compressor Stall/Hammershock Time Histories

The Mach 2.5 40-60 inlet has also been used to study the hammershock/compressor stall response both experimentally and computationally. During inlet unstart, an overpressure may exist in the vicinity of the normal shock as a hammershock is formed. In the experiment a plug at the end of the inlet duct was cycled to produce a transient of known magnitude and frequency. High speed pressure transducers at several locations through the inlet then recorded the inlet's response to the downstream transient. The large perturbation analysis was also used to model this problem with the downstream transient provided as a boundary condition. The comparison of the analysis and experiment show that the analysis can accurately predict the magnitude of the unstart transient with the hammershock present. The time history of the analysis does not agree with the experiment probably because of the one-dimensional nature of the analysis.

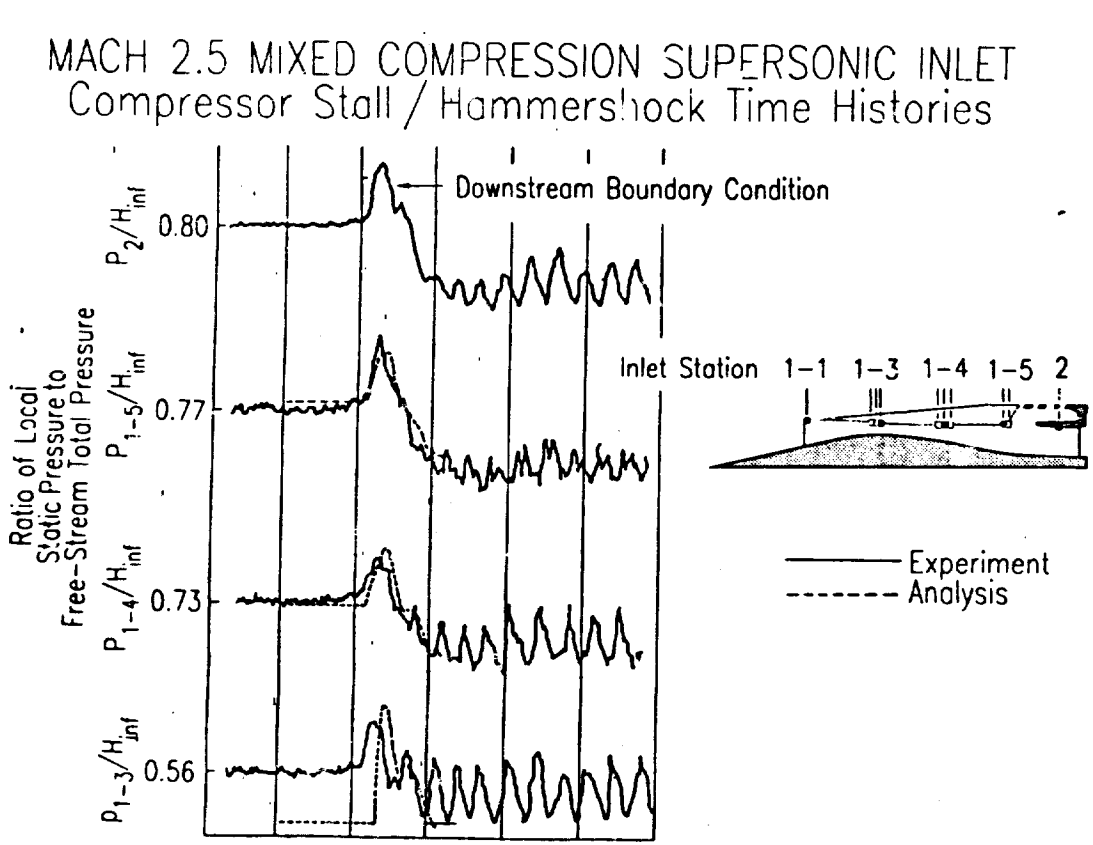

SEQUENTIAL MACH NUMBER CONTOURS

Inlet Buzz

Details of the inlet buzz problem are being studied using a time accurate, unsteady Navier-Stokes solver. These calculations were completed by Newsome (Ref. 59) at Wright-Patterson AFB using a MacCormack explicit scheme. The problem involves flow through an axisymmetric inlet at free stream Mach 2.0. A sequence of Mach contours plots covering one cycle of the buzz is shown in the figure. The bow shock was forced to the tip of the centerbody as a result of interaction with a reflected compression wave. In the expulsion phase, from t=.159e-01 to .175e-01 sec, a region of reverse flow extended between the base of the bow shock and the cowl lip. The shear layer dividing the two regions is clearly visible. As the shock reached the centerbody tip, the shear layer ruptured and flow spilled radially outward. The bow shock remained in this position for a period of time corresponding to the propagation and reflection of an expansion wave. At this time, t=.199e-01 sec, the inlet began to ingest mass and the shock retreated to a position just forward of the cowl lip. In this phase, t=.215e-01 to .239e-01 sec, several regions of separated flow, located on the centerbody and cowl in alternating fashion, are clearly visible immediately downstream from the cowl lip. The pattern then repeates itself as it did in the experiment.

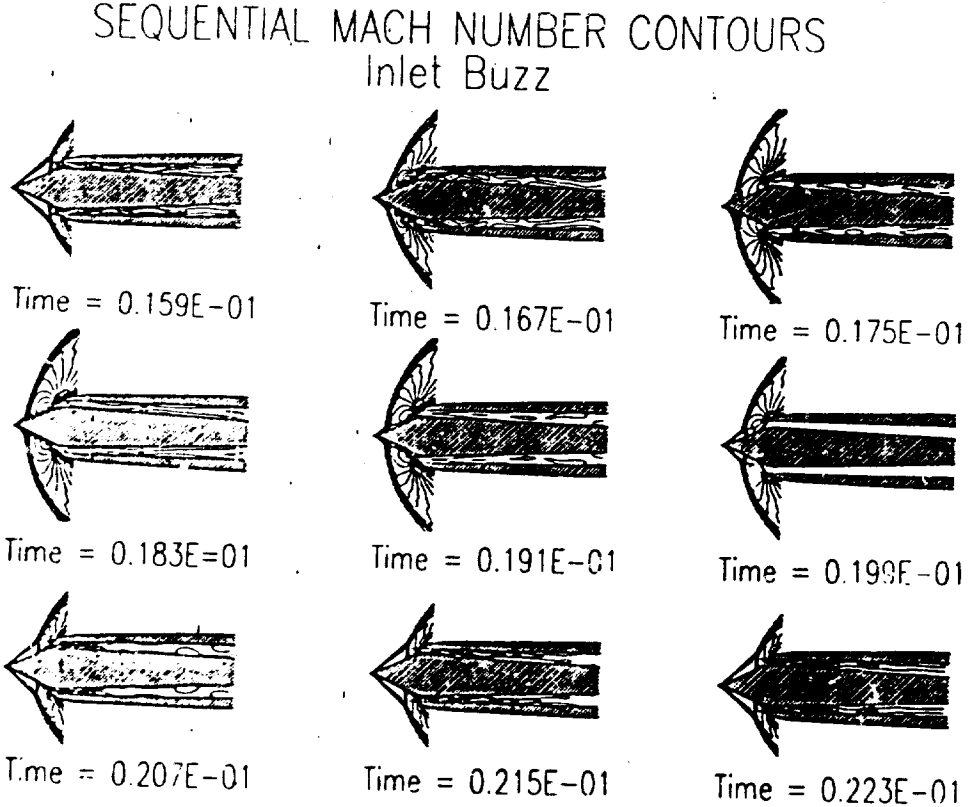

GENERIC HYPERSONIC VEHICLE

Scramjet Engine Module

As inlets and engines are designed for hypersonic speeds, additional physical problems are encountered. The stagnation pressure and temperatures are so high, and the losses through shock waves so great that one must develop some kind of supersonic combustion engine to avoid bringing the flow to subsonic conditions. The inlet then becomes a variation of the mixed compression inlet with no terminal normal shock. To take advantage of the compression field provided by the bow shock of the aircraft, hypersonic inlets are highly integrated with the airframe. Because of the heat generated along the body surface, hypersonic inlets must operate without boundary layer bleed; the hot external flow must not be taken inside the vehicle. Hypersonic inlet usually are designed with a minimum of variable geometry also to avoid problems associated with sealing moving surfaces. Inlet design remains a major challenge for hypersonic air-breathing propulsion.

Hypersonic flows are characterized by high Mach numbers in the inviscid regions, high gradients in the vicinity of shock waves or solid surfaces, and thick, heated boundary layers. To accurately model the high gradients near shocks and along surfaces, one must employ large numbers of mesh points in the calculation. Most flow calculations in this regime encounter some degree of post-shock flow oscillations, which can be minimized either through some form of artificial viscous damping or through the use of increased grid resolution. To accurately model the high temperatures found in hypersonic flows, one needs to include real-gas effects in the energy equation models. This model can take several forms from the simplest specific heats as a function of temperature to the more complex chemical kinetic and specie models. To accurately model the thick boundary layers present in hypersonic flows, one may need to consider a variety of turbulence and transition models.

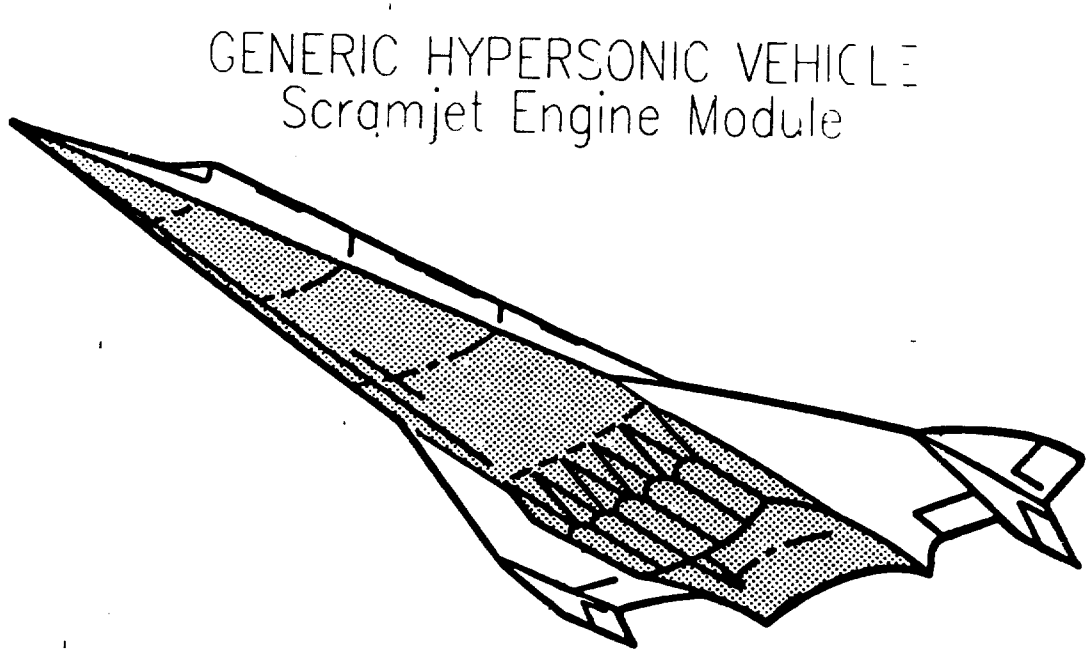

SCRAMJET INLET MODULE

Static Pressure Contours

Minf=3.5

The following three figures show calculated results for the flow through a hypersonic inlet at off-design conditions. The full Navier-Stokes calculations were performed on a supercomputer at NASA Langley by Kumar (Ref. 60) on geometries which were tested in the Langley hypersonic wind tunnels. The first figure shows static pressure contours through the center of the inlet for three different conditions; inviscid, laminar and turbulent flows. The inlet has compression wedges both top and bottom and one sees evidence of shock and expansion fans being generated by the compression surfaces. This shock system moves slightly upstream as the viscous effects are considered because of displacement effects within the boundary layer.

SCRAMJET INLET MODULE
Static Pressure Contours
Minf = 3.5

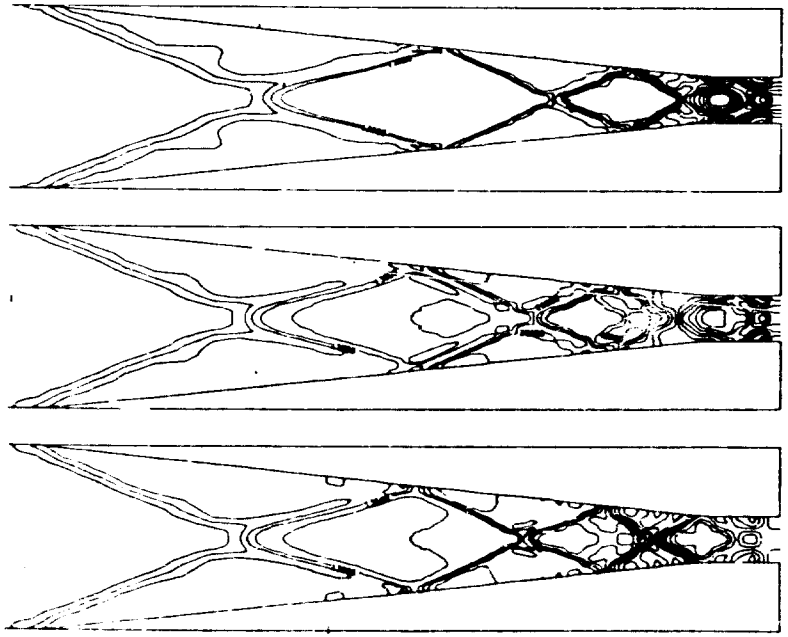

SCRAMJET INLET MODULE

Velcoity Vector Field

Minf=3.5

This figure, like the previous figure, shows flow through a hypersonic inlet at off-design conditions. Shown here are velocity vector plots for the inviscid, laminar and turbulent flow through this inlet. Both the laminar and turbulent cases indicate boundary layer growth on the compression surfaces. In the laminar case, flow separation occurs at the shock reflection locations, while in the turbulent calculation, no separation is seen. The turbulent boundary layer is able to accept higher adverse pressure gradients than the laminar without separating.

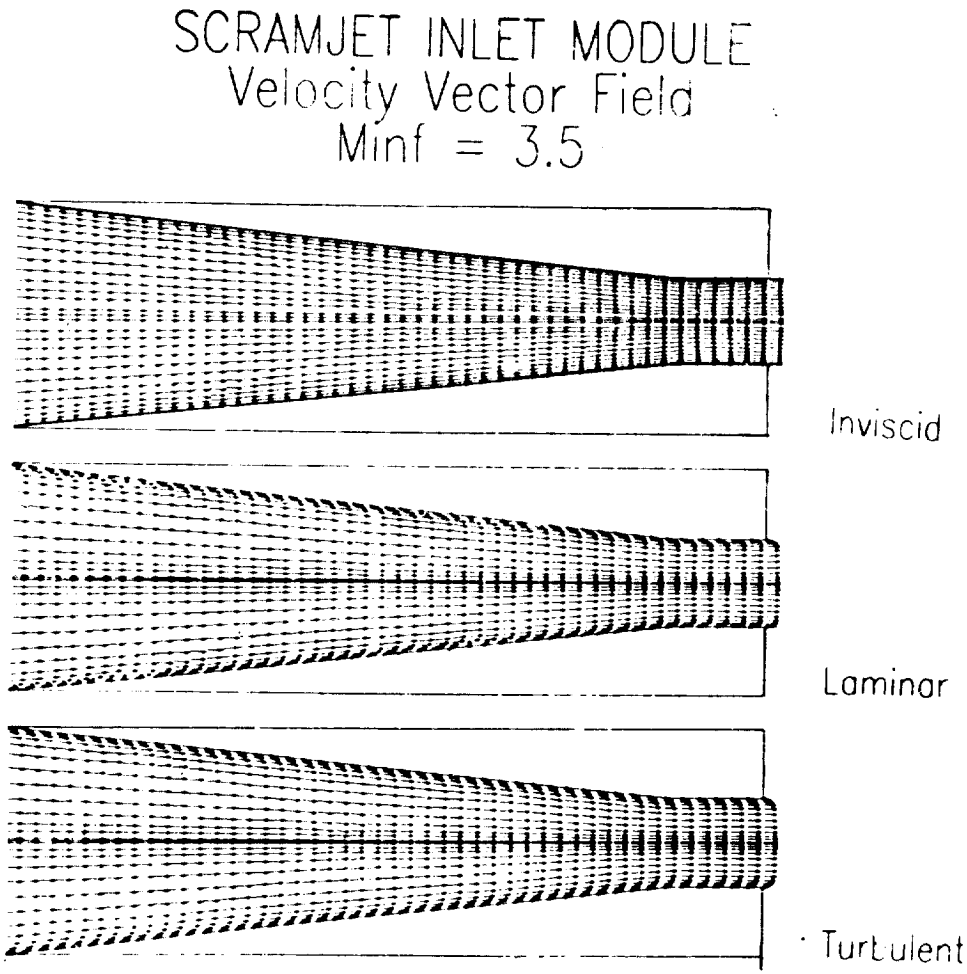

SCRAMJET INLET MODULE

Sidewall Static Pressure Distribution

This figure shows the sidewall pressure distribution at two heights in the hypersonic inlet. Experimental results are also shown in this figure. One can see large differences in the inviscid, laminar and turbulent pressure distributions especially between x/H = 2.6 to 3.5. For example, the inviscid pressure distribution shows substantial decrease in pressure due to sidewall expansion around x/H = 3.1, but the laminar flow does not see this expansion due to thickening boundary layer caused by flow separation near x/H = 3.1. The flow in the region between x/H =2.6 and 3.5 is highly complex due to the interactions of sidewall shock, sidewall expansion, cowl shock, expansion due to end effects and induced shocks due to flow separation. All of these interactions are taking place in a region where the gap between the sidewalls is relatively small. Even with all these complexities, the predicted results agree reasonably well with experimental data.

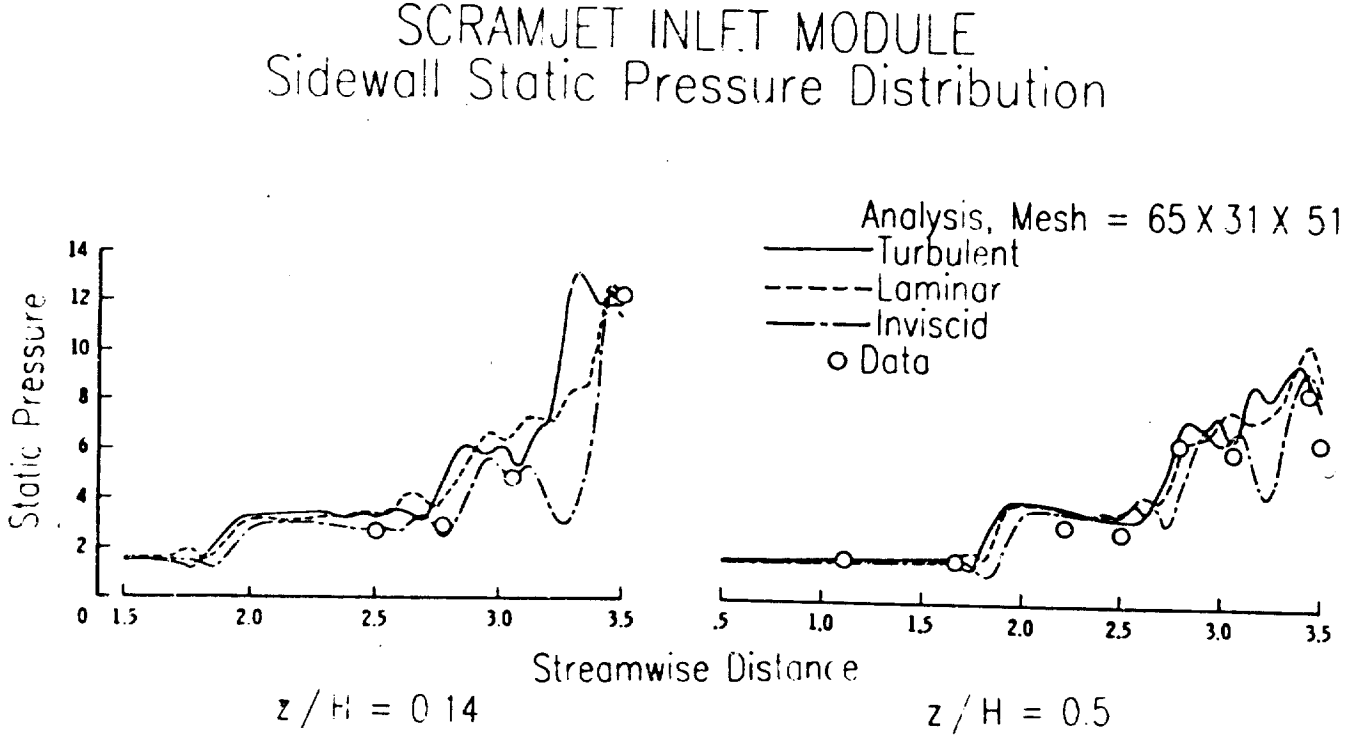

MACH 7.4 HYPERSONIC INLET

CFD Validation Configuration

Effect of Mesh Points

Several calculations have been made of the flow through a Mach 7.4 inlet and the results of the calculations have been compared to experimental results. The hypersonic inlet to be calculated was originally tested at NASA Ames (Ref. 25) and the analysis done at NASA Lewis using a PNS solver (Ref. 61). At Mach 7.4 the nominal 6.5 degree wedge produces a Mach 6.0 flow at the entrance to the inlet. A shock is generated by the cowl lip and this shock traverses the internal flow passage and is reflected by the ramp surface. In the vicinity of the shock reflection, the flowfield was surveyed with a traversing pitot pressure probe to obtain pressure profiles throughout the inlet. By varying the grid resolution and turbulence models in the calculations, the sensitivity to these factors can be assessed. These answers can then aid future calculations in this speed regime and beyond.

In each figure a schematic of the inlet is shown at the top and a comparison of the calculated and experimental pitot pressure profiles is shown at the bottom. The location of the profiles are noted on the upper schematic. In all cases the results of the analysis are given by solid or dashed lines, while the experimental results are noted by the circles. In all of the calculations, the free stream conditions were set to the experimental tunnel conditions of Mach number equal to 7.4, total pressure equal 4.14E06 Newtons per meter squared and total temperature equal to 811 degrees Kelvin. All of the calculations were run fully turbulent, although there was some indication in the test that transition occurs on both ramp and cowl surfaces.

Considering the profile at the left, the lower part of the figure shows the thick boundary layer which has grown on the ramp surface; the thickness is indicated by the location where the curve turns verticle. Continuing up the curve, the sharp turn to the right is indicitive of the cowl shock location while the gradual rise to the right and up is caused by the distributed compression on the inside of the cowl. Near the top of the curve, it turns quickly back to the left which indicates the thickness of the boundary layer on the cowl. In general, the comparison between analysis and experiment is excellent; the shock location and strength has been correctly modelled, as has the thickness of the ramp boundary layer. The boundary layer on the cowl is thinner than the calculated results because of laminar to turbulent transitioning effects.

The two calculations of this figure have been run with different numbers of mesh points in the direction normal to the ramp and cowl surfaces. When one hundred mesh point are used, the flow experiences severe post-shock pressure oscillations which are most evident in the middle profile dashed curve. Other researchers have experienced these oscillations in high speed flow calculations particularly when central differencing techniques are used. While others are attempting to overcome these numerical problems with special differencing schemes, or various types of artificial damping, this study indicates that the problem can be overcome with increased mesh resolution. This is shown by the smooth solid curves which used three hundred mesh points in the normal direction. Obviously, some trade studies must be performed on the increased run time with increased resolution versus shock smearing with artificial damping.

MACH 7.4 HYPERSONIC INLET
CFD Validation Configuration
Effect of Mesh Points

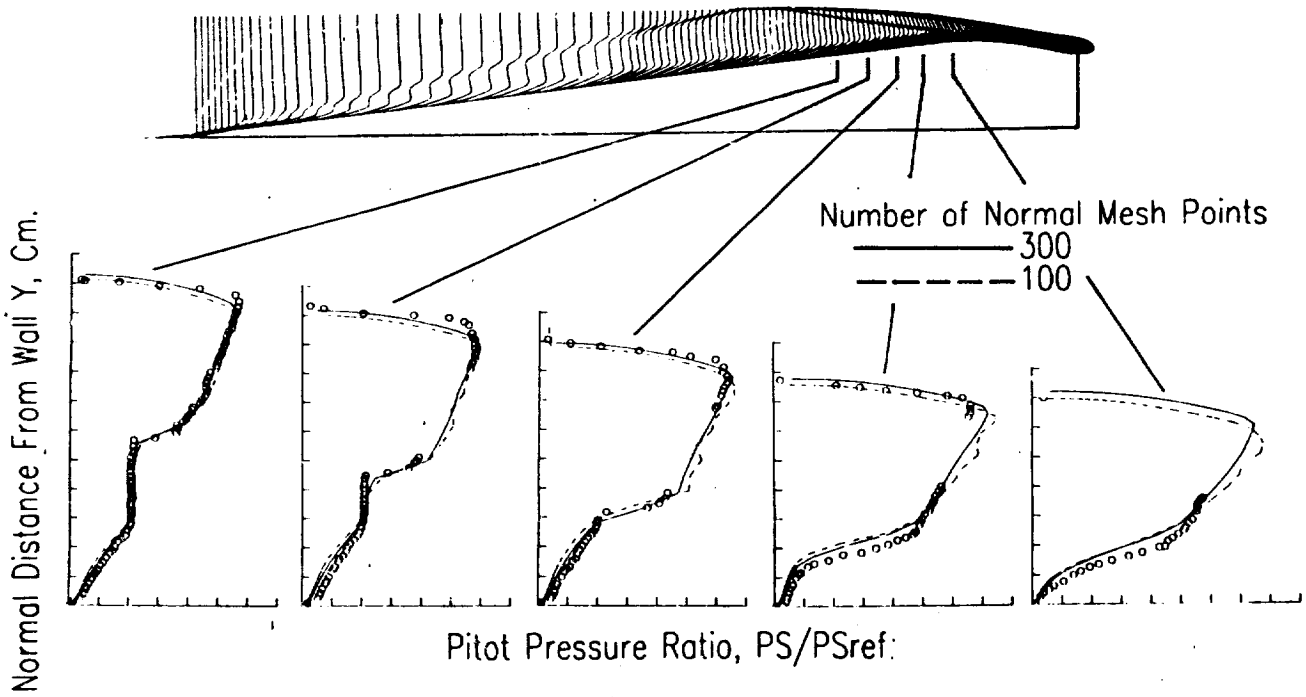

MACH 7.4 HYPERSONIC INLET

CFD Validation Configuration

Effect of Turbulence Model

The results of two calculations of the Mach 7.4 inlet employing different length scales in the turbulence model are shown here. The dashed line shows the results using a McDonald-Camarata model which has been successfully used in the PNS code for many different types of problems in the low supersonic speed regime. For the hypersonic calculations, however, this model breaks down. Bushnell and Beckwith (Ref. 62) found similar problems with this model in their earlier research. and using a length scale model based on this work, the results appear as the solid lire. The comparison with experiment is much better and the improved model is recommended for calculation of hypersonic flows. This calculation indicates possible dangers in the calculation of high speed flows for which no comparison with experimental data is available; a turbulence model which works quite well at lower speeds gives erroneous results for higher Mach number flows.

MACH 7.4 HYPERSONIC INLET
Effect of Mesh Resolution
Streamwise Velocity

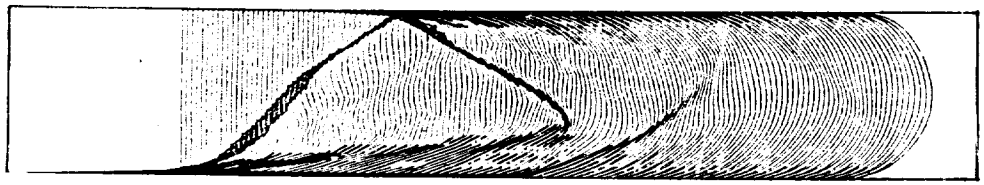

100 Normal Mesh Points

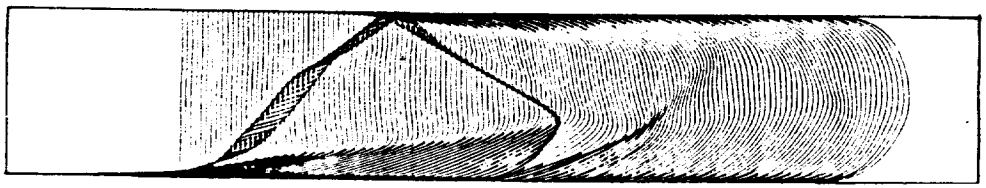

300 Normal Mesh Points

MACH 7.4 HYPERSONIC INLET
CFD Validation Configuration
Effect of Turbulence Models

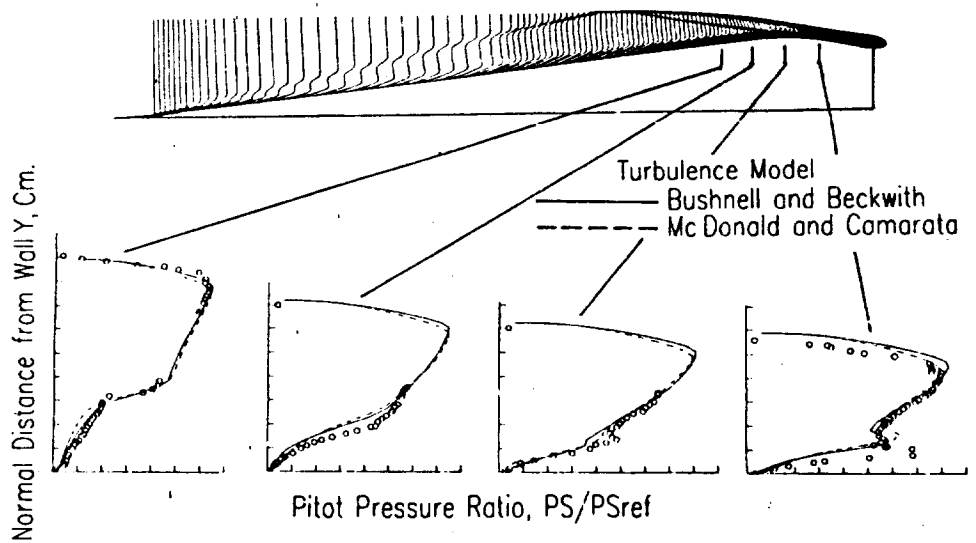

MACH 7.4 HYPERSONIC INLET
Effect of Mesh Resolution
Normal Velocity

This figure demonstrates the effects of mesh resolution on the Mach 7.4 inlet calculation in a different way than the previous figure. Plotted here are profiles of the velocity perpendicular to the stream direction which have been normalized to the local flow passage height. This component of the velocity is the most sensitive to local variations in pressure. The upper part of the figure shows the computed results with one hundred grid points between the ramp and cowl surface, while the bottom has three hundred points. The bottom figure is much smoother than the top figure indicating better resolution of flow phenomenon in the three hundred point case and elimination of numerical oscillations with increased grid resolution.

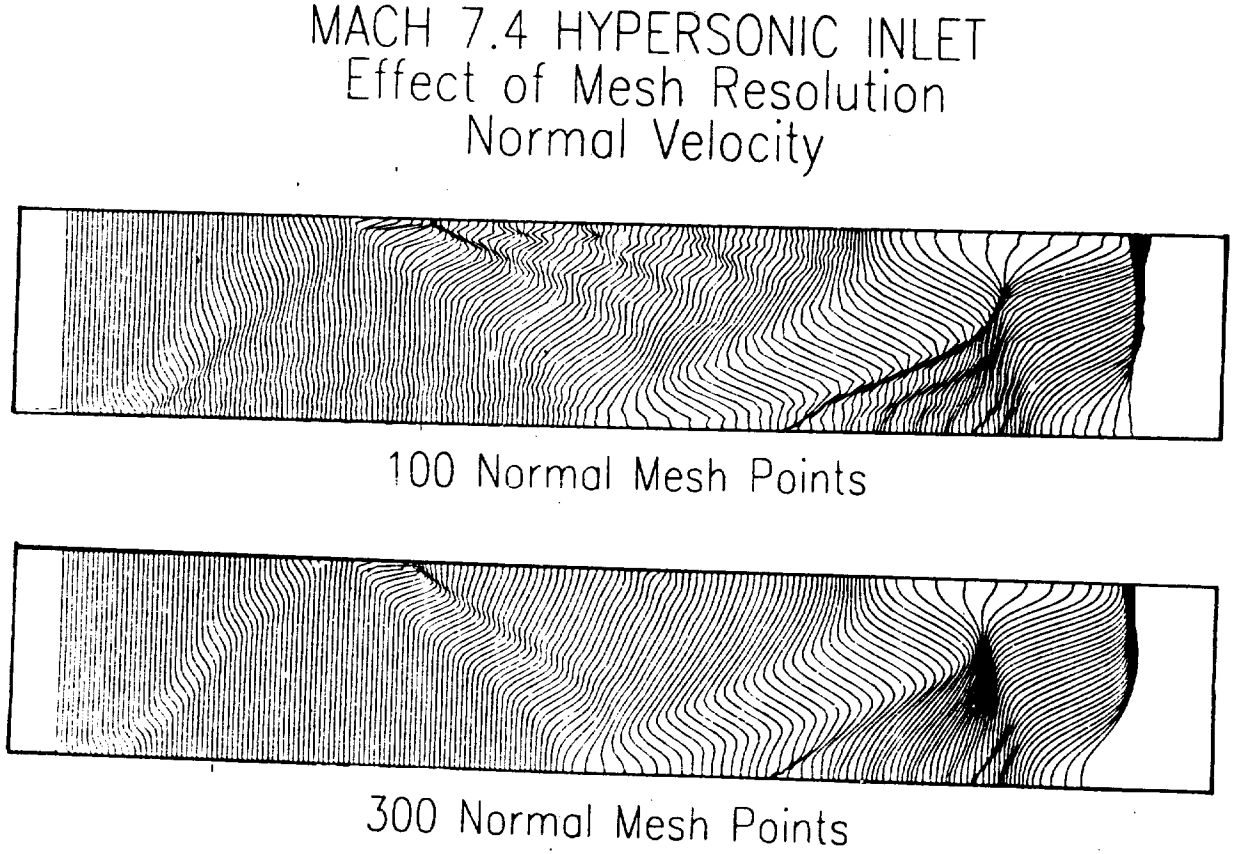

3D HYPERSONIC CORNER INTERACTION

The three dimensional PNS analysis is also being used to identify selected benchmark phenomenon that will become important in the design of advanced aircraft inlet concepts. These highly three dimensional shock wave turbulent boundary layer interactions center around the hypersonic corners interaction of Cresci (Ref. 32).

The primary interest in the experiment was directed towards the hypersonic, low density flow regime wherein the inviscid shock layer and the viscous boundary layer produced under these conditions are of the same order of magnitude. In this case, the viscous and inviscid effects are interrelated and cannot be treated independently. This phenomena is important in that it represents a complex corner interaction that is typical of a large class of problems associated with advanced supersonic inlet concepts. The structure of the corner flow interaction is shown in this figure and consists of an oblique corner shock resulting from the intersection of the shock waves generated by the rapid boundary layer growth on the wall surfaces, and a set of two tripple points formed by intersection of the embedded shock wave system. This interaction was studied by Buggeln, McDonald and Kim (Ref. 5), using the PEPSIS forward marching three dimensional flow solver, as part of the benchmark verification process. The model was mounted in a Mach 11.8 blowdown wind tunnel, and tests were conducted at free stream Reynolds number varying between 0.15E6 and 0.5E6. The tunnel stagnation temperature varied between 1700 degrees Rankine and 1900 degrees Rankine which produced wall temperature ratios of 0.29 and 0.32. Calculations were performed on the hypersonic corner interaction using a grid system composed of 50X50X120 (300,000) points. Although the calculations were performed on the Lewis IBM 370/3033, the equivalent computing time on the Lewis CRAY I computer would be 10.8 CPU minutes. The next three figures present the calculated Mach number, static pressure, and total pressure field of the hypersonic corner interaction. The primary features of an oblique corner shock wave generated by the intersection of the the boundary layer shock wave from the wall surfaces and the set of triple points formed by the embedded shock system are easily seen in these figures. In addition, the secondary feature of a triangular region bounded by two slip surfaces and the corner shock wave was also revealed in the calculations.

HYPERSONIC CORNER INTERACTION
Shock Wave Boundary Layer Structure

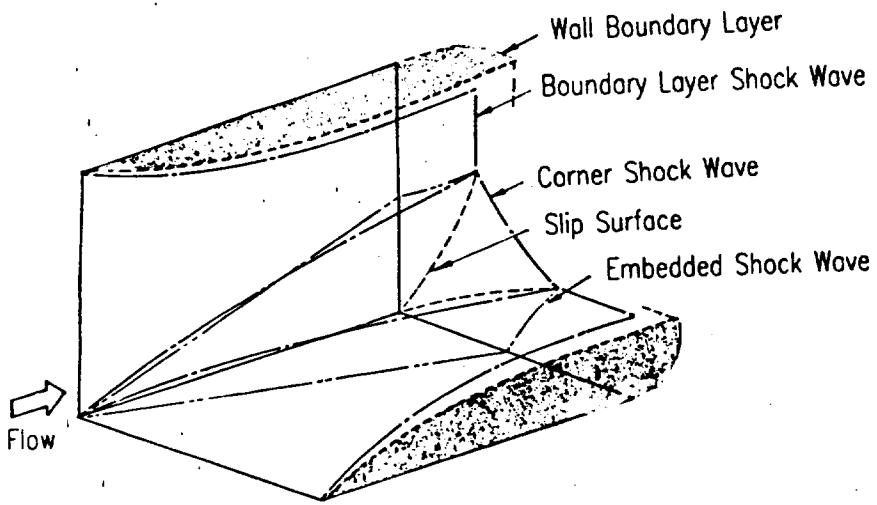

HYPERSONIC CORNER INTERACTION
Minf = 11.8, Laminar Flow, Rey = 0.5×10^6
Mach Number Contours

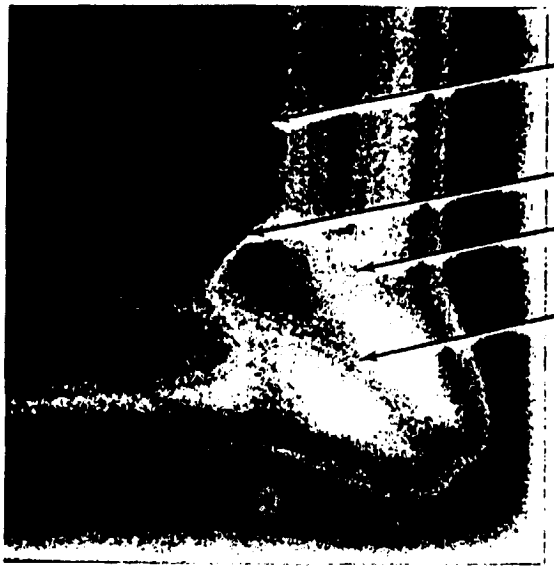

HYPERSONIC CORNER INTERACTION
Minf = 11.8, Laminar Flow, Rey = 0.5×10^6
Static Pressure Contours

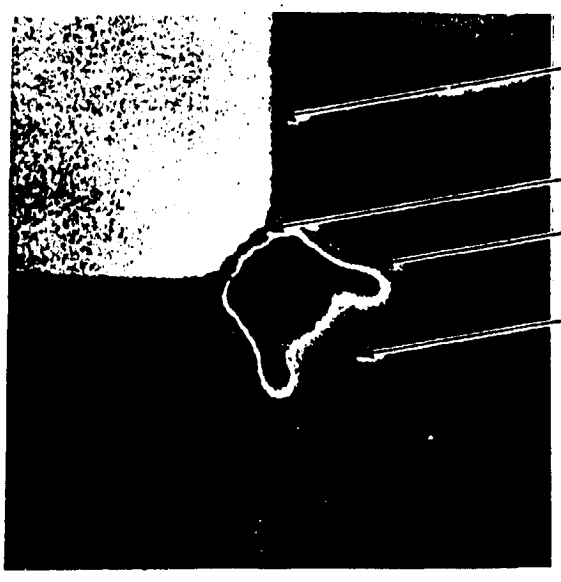

HYPERSONIC CORNER INTERACTION
Minf = 11.8, Laminar Flow, Rey = 0.5×10^6
Total Pressure Contours

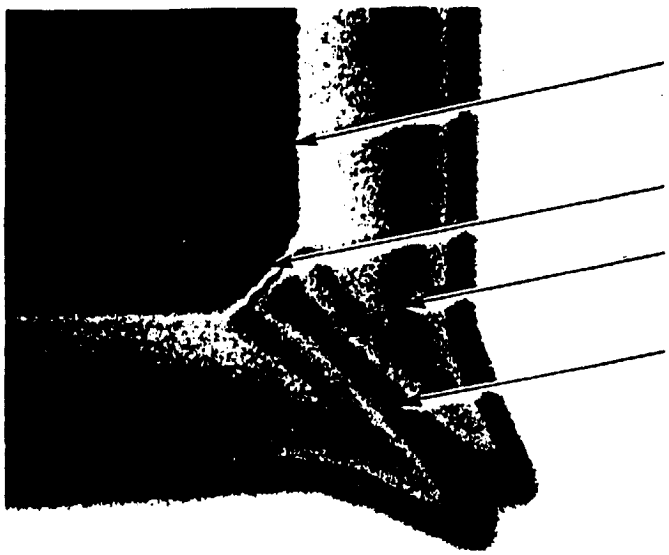

HYPERSONIC CORNER INTERACTION
Minf = 11.8, Laminar Flow, Rey = 0.5×10^6
Static Temperature Contours

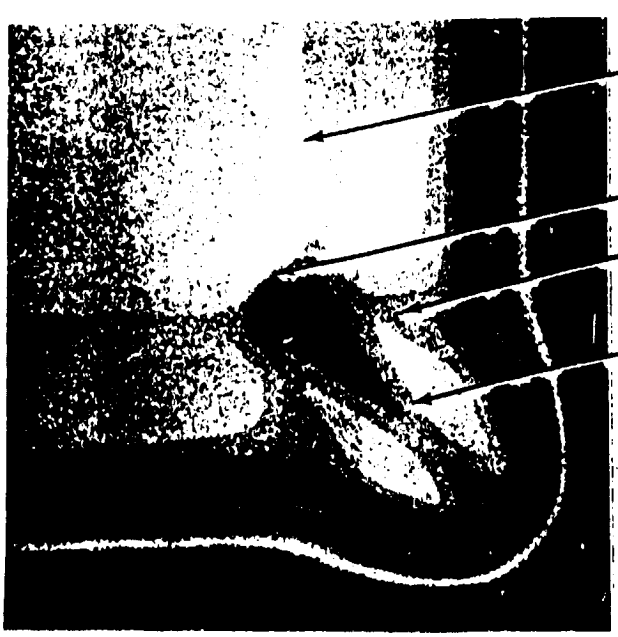

CFD FOR INLET AIRFRAME INTEGRATION

A Future Perspective

CFD for Inlet Airframe Integration has opened a new realm of capability for the design engineer in that, for the first time in history, the intricate features of complex flow can be computed. This new capability in turn has set the stage for new levels of understanding of the fluid flows, once the the researcher or designer is satisfied that the codes numerical algorithm and physical modeling accurately represent the critical physics of the flow. This confidence can only be gained by detailed comparison with experimental data of sufficient accuracy and detail to verify the CFD capability. These typres of experiments are call "Benchmark" or "Validation" experimemts, and affords the researcher the opportunity to study and understand the highly complex three dimensional viscous flows from a building block concept. Thus CFD has introduced "Analysis Based Design" into the design system, where analysis and fundamental understanding replaces trial-and-error and "Matrix Testing".

With close interaction between CFD and experimentation, advanced computer programs will be used both to design an experiment and to predict the results so that the the test. or design, is under control at all times, But this interaction also gives the researcher a fundamental understanding of the fluid processes that are important to the inlet airframe system under design. This is the main idea of this seminar series on a "User's Technology Guide to CFD Inlet Airframe Integration".

CFD FOR INLET AIRFRAME INTEGRATION
A Future Perspective

"With close interplay of CFD and experimentation, advanced computer programs will be used both to design an experiment and predict the results so that the test (or design) is under control at all times"

Current Capabilities and Future Direction
in
Computational Fluid Dynamics

REFERENCES AND BIBLIOGRAPHY

1. McDonald, H. and Briley, W. R., "Three-Dimensional Supersonic Flow of a Viscous or Inviscid Gas," J. Comp. Phys., Vol. 19, pp. 150-178, October 1975.

2. Buggeln, R. C., McDonald, H., Levy, R. and Kreskovsky, J. P., "Development of a Three Dimensional Supersonic Inlet Flow Analysis," NASA CR-3218, January 1980.

3. Buggeln, R. C., McDonald, H., Kreskovsky, J. P. and Levy, R., "Computation of Three Dimensional Supersonic Flow in Inlets," AIAA Paper No. 80-0194, January 1980.

4. Buggeln, R. C., McDonald, H. and Kim, Y. W., "Computation of Multi-Dimensional Viscous Supersonic Flow by Spatial Forward Marching," AIAA Paper No. 83-0177, January 1983.

5. Buggeln, R. C., McDonald, H., and Kim, Y. W., "Computation of Multi-Dimensional Viscous Flow by Spatial Forward Marching," (NASA CR in preparation).

6. Briley, W. R. and McDonald, H., "Solution of the Multidimensional Compressible Navier Stokes Equations by a Generalized Implicit Method," J. Comp. Phys., Vol. 24, p. 372, August 1977

7. Briley, W. R. and McDonald, H., "On the Structure and Use of Linearized Block Implicit Schemes," J. Comp. Phys., Vol. 34, January 1980.

8. McDonald, H. and Briley, W. R., "Computational Fluid Dynamic Aspects of Internal Flows," AIAA Paper No. 79-1445, July 1979.

9. McDonald, H., Shamroth, S., and Briley, W. R., "Transonic Flow with Viscous Effects," Transonic, Shock and Multidimensional Flows, Academic Press, 1982.

10. Douglas, J. and Gunn, J. E., "A General Formulation of Alternating Direction Methods Part I Parabolic and Hyperbolic Problems," Numerishe Math., Vol. 6, July 1964.

REFERENCES AND BIBLIOGRAPHY

11. Briley, W. R., "Numerical Method for Predicting Three-Dimensional Steady Viscous Flow in Ducts," J. Comp. Phys., Vol. 14, pp. 8-28, January 1974.

12. Eiseman, P. R., McDonald, H. and Briley, W. R., "A Method for Computing Three-Dimensional Viscous Diffuser Flows," UARL Report R75-911737, July 1975.

13. Roscoe, D. V., Shamroth, S. J., Gibeling, H. J., and McDonald, H., Investigation of the Mechanism of Transonic Shock Wave/Boundary Layer Interactions Using a Navier Stokes Analysis," SRA Rep. R83-930006-F, October 1983.

14. Liu, N. S., Shamroth, S. J., and McDonald, H., "Numerical Solution of the Navier-Stokes Equations for Compressible Turbulent Two/Three Dimensional Flows in the Terminal Shock Region of an Inlet/Diffuser," AIAA Paper No. 83-1892, July 1983.

15. Liu, N. S., Shamroth, S. J., and McDonald, H., "Numerical Solution of the Navier-Stokes Equations for Compressible Turbulent Two/Three Dimensional Flows in the Terminal Shock Region of an Inlet/Diffuser," NASA CR 3723, August 1983.

16. Liu, N. S., Shamroth, S. J., and McDonald, H., "Dynamic Response of Shock Waves in 2-D Transonic Diffuser and Supersonic Inlets," (Report in preparation).

17. Briley, W. R., Kreskovsky, J. P., and McDonald, H., "Computation of Three-Dimensional Viscous Flow in Straight and Curved Ducts," UTRC Report R76-911841, August 1976.

18. Eiseman, P. R., Levy, R., McDonald, H., and Briley, W. R., "Development of a Three Dimensional Turbulent Duct Flow Analysis," NASA CR 3029, November 1978.

19. Levy, R., McDonald, H., Briley, W. R., and Kreskovsky, J. P., "A Three-Dimensional Turbulent Compressible Subsonic Duct Flow Analysis for Use with Constructed Coordinate Systems," NASA CR 3389, April 1981.

20. Levy, R., Briley, W. R., and McDonald, H., "Viscous Primary/Secondary Flow Analysis for Use with Nonorthogonal Coordinate Systems," AIAA Paper No. 83-0556, January 1983.

REFERENCES AND BIBLIOGRAPHY

21. Briley, W. R., and McDonald, H., "Analysis and Computation of Viscous Subsonic Primary and Secondary Flows," AIAA Paper No. 79-1453, July 1979.

22. Fukuda, M. K., Hingst, W. R. and Reshotko, E., "Control of Shock-Wave Boundary Layer Interactions by Bleed in Supersonic Mixed Compression Inlets," NASA CR 2595, August 1975.

23. Anderson, W. E. and Wong, N. D., "Experimental Investigation of a Large Scale, Two-Dimensional, Mixed-Compression Inlet System - Performance at Design Conditions, M=3.0," NASA TM X-2016, May 1970.

24. Syberg, J., and Hickcox, T. E., "Design of a Bleed System for a Mach 3.5 Inlet," NASA CR 2187, January 1973.

25. Gnos, A. V. and Watson, E. C., "Investigation of Flow Fields within Large-Scale Hypersonic Inlet Models," NASA TN D-7150, April 1973.

26. Rose, W. C., "Behavior of a Compressible Turbulent Boundary Layer in a Shock Wave Induced Adverse Pressure Gradient," PhD Thesis, Univ. of Washington, 1972. Also NASA TN D-7092, March 1973.

27. Oskam, B., Vas, I. E. and Bogdonoff, S. M., "Mach 3.0 Oblique Shock Wave/Turbulent Boundary Layer Interaction in Three Dimensions," AIAA Journal, Vol. 16, No. 10, pp. 1090-1096, December 1976.

28. Oskam, B., Vas, I. E. and Bogdonoff, S., "Oblique Shock Wave/Turbulent Boundary Layer Interaction at Mach 3.0," AFFDL-TR-76-48, Part I, June 1976.

29. Oskam, B., Vas, I. E. and Bogdonoff, S., "Oblique Shock Wave/Turbulent Boundary Layer Interaction at Mach 3.0," AFFDL-TR-76-48, Part II, March 1978.

30. Rainbird, W. J., "Turbulent Boundary Layer Growth and Separation on a Yawed Cone," AIAA Journal, pp 2410-2416, December 1968.

REFERENCES AND BIBLIOGRAPHY

31. Hingst, W. R. and Tanji, F. T., "Experimental Investigation of a Two-Dimensional Shock-Turbulent Boundary Layer Interaction with Bleed," NASA TM 83057, (Also AIAA Paper No. 83-0135), January 1983.

32. Cresci, R. J., "Hypersonic Flow along Two Intersecting Planes," AFOSR Report 66-0500, March 1966.

33. West, J. E., and Korkegi, R. H., "Supersonic Interaction in the Corner of Intersecting Wedges at High Reynolds Numbers," AIAA Journal, Vol 10, No. 5, pp 652-656, May 1972.

34. Settles, G. S., Perkins, J. J., and Bogdonoff, S. M., "Upstream Influence Scaling of 2D & 3D Shock/Turbulent Boundary Layer Interactions at Compression Corners," AIAA Paper No. 81-0334, January 1981.

35. Anderson, B. H. and Towne, C. E., "Numerical Simulation of Supersonic Inlets Using a Three-Dimensional Viscous Flow Analysis," NASA TM 81411, (Also AIAA Paper No. 80-03840), January 1980.

36. Anderson, B. H., and Benson, T. J., "Numerical Solution to the Glancing Sidewall Oblique Shock Wave/Turbulent Boundary Layer Interaction in Three Dimensions," NASA TM 83056, (Also AIAA Paper No. 83-0136), January 1983.

37. Benson, T. J., and Anderson, B. H., "Validation of a Three-Dimensional Viscous Analysis of Axisymmetric Supersonic Inlet Flow Fields," NASA TM 85038, (Also AIAA Paper No. 83-0135), January 1983.

38. Mateer, G. G., and Viegas, J. R., "Effect of Mach and Reynolds Number on a Normal Shock-Wave/Turbulent Boundary Layer Interaction," AIAA Paper No. 79-1502, July 1979.

39. Bogar, T. J., Sajben, M., and Kroutil, J. C., "Characteristic Frequency and Length Scale in Transonic Diffuser Flow Oscillation," AIAA Paper No. 81-1291, 1981.

40. Salmon, T. J., Bogar, T. J., and Sajben, M., "Laser Velocimeter Measurements in Unsteady, Separated, Transonic Diffuser Flows," AIAA Paper No. 81-1197, 1981.

REFERENCES AND BIBLIOGRAPHY

41. Sajben, M., Bogar, T. J., and Kroutil, J. C., "Forced Oscillation Experiments in Supercritical Diffuser Flows with Application to Ramjet Instabilities," AIAA Paper No. 81-1487, 1981.

42. Briley, W. R., Buggeln, R. C., and McDonald, H., "Computation of Laminar and Turbulent Flow in 90 Degree Square Duct and Pipe Bends Using the Navier-Stokes Equations," SRA Rpt. R82-920009, 1982.

43. Rowe, M., "Measurements and Computations of Flow in Pipes," J. Fluid Mech., Vol. 43, p. 771-783, 1970.

44. Taylor, A. M. K. P., Whitelaw, J. H. and Yianneskis, M., "Measurement of Laminar and Turbulent Flow in a Curved Duct with Thin Inlet Boundary Layers," NASA CR 3367, January 1981.

45. Enayet, M. M., Gibson, M. M., Taylor, A. M. K. P., and Yianneskis, M., "Laser Doppler Measurements of Laminar and Turbulent Flow in a Pipe Bend," NASA CR 3551, May 1982.

46. Agrawal, Y., Talbot, L and Gong, K., "Laser Anemometer Study of Flow Development in Curved Circular Pipes," J. Fluid Mechanics, Vol. 85, pp 497-518, 1978.

47. Taylor, A. M. K. P., Whitelaw, J. H., and Yianneskis, M., "Developing Flow in S-Shaped Ducts, Part I-Square Cross Section Ducts," NASA CR 3550, May 1982.

48. Taylor, A. M. K. P., Whitelaw, J. H., and Yianneskis, M., "Developing Flow in S Shaped Ducts Part II: Circular Cross-Section Duct," (NASA CR in preparation).

49. Bansod, P., and Bradshaw, P., "The Flow in S-Shaped Ducts," Aeronautical Quarterly, vol. 23, pp 131-140, May 1972.

50. Taylor, A. M. K. P., Whitelaw, J. H., and Yianneskis, M., "Turbulent Flow in a Square-to Round Transition," NASA CR 3447, July 1981.

REFERENCES AND BIBLIOGRAPHY

51. Vakili, A., Wu, J. M., Hingst, W. R., and Towne, C. E., "Comparison of Experimental and Computational Compressible Flow in an S-Duct," AIAA Paper No. 84-903, January 1984.

52. Towne, C. E., and Anderson, B. H., "Numerical Simulation of Flows in Curved Diffusers with Cross-Sectional Transitioning Using a Three-Dimensional Viscous Analysis," NASA TM 81672, (Also AIAA Paper No. 81-0003), January 1981.

53. Towne, C. E., "Computations of Viscous Flow in Curved Ducts and Comparison with Experimental Data," AIAA Paper No. 84-0531, January 1984.

54. Anderson, B. H., Putt, C. W., and Giamati, C. C., "Application of Computer Generated Color Graphic Techniques to the Processing and Display of Three Dimensional Fluid Dynamic Data," NASA TM 82658, November 1981.

55. Anderson, B. H., Putt, C. W., and Giamati, C. C., "Fluid Dynamic Data-In Color and Three Dimensions," Mechanical Engineering, pp. 30-35, March 1982.

56. Vakili, A. D., Wu, J. M., Liver, P., and Bhat, M. K., "Experimental Investigation of Secondary Flow in a Diffusing S-Duct," (Warren Hingst Project Manager, NASA Lewis Research Center, to be published), 1986

57. Campbell, A.F., and Forester, C.K., "Evaluation of a Method for Analyzing the Aperture Region of Two-Dimensional External Compression Inlets", AIAA Paper No. 85-3072, October 1985.

58. Howlett, D.G. and Hunter, L.G., "A Study of a Supersonic Axisymmetric Spiked Inlet at Angle of Attack Using the 3-D Navier Stokes Equations", AIAA Paper No. 86-0308, January 1986.

59. Newsome, R.W., "Numerical Simulation of Near-Critical and Unsteady Subcritical Inlet Flow Fields," AIAA Paper No. 83-0175, January 1983.

60. Kumar, Ajay, "Numerical Analysis of a Scramjet Inlet Flow Field Using the Three-Dimensional Navier-Stokes Equations," JANNAF Propulsion Meeting, February 1983.

REFERENCES AND BIBLIOGRAPHY

61. Kunik, W.G., Benson, T.J., Ng, W-F, and Taylor, A., "Two- and Three-Dimensional Viscous Computations of a Hypersonic Inlet Flow," AIAA Paper No. 87-0283, January 1987.

62. Bushnell, D.M., and Beckwith, I.E., "Calculation of Nonequilibrium Hypersonic Turbulent Boundary Layers and Comparisons with Experimentl Data," AIAA Journal Vol. 8, No. 8, pp 1462-1469,

63. Current Capabilities and Future Direction in Computational Fluid Dynamics," National Acadamy Press, Washington, D.C., 1986

64. Anderson, B. H.: "Three Dimensional Viscous Design Methodology of Supersonic Inlet Systems for Advanced Technology Aircraft", AIAA 84-0194, 1984. August 1970.